Senescence marker protein 30 functions as gluconolactonase in L-ascorbic acid biosynthesis, and its knockout mice are prone to scurvy

Yoshitaka Kondo*†‡, Yoko Inai‡§, Yasunori Sato*‡¶, Setsuko Handa*, Sachiho Kubo*, Kentaro Shimokado†, Sataro Goto¶, Morimitsu Nishikimi§‖, Naoki Maruyama*, and Akihito Ishigami*,**

*Department of Molecular Pathology, Tokyo Metropolitan Institute of Gerontology, Tokyo 173-0015, Japan; †Vascular Medicine and Geriatrics, Tokyo Medical and Dental University, Tokyo 113-8510, Japan; §Department of Biochemistry, Wakayama Medical University, Wakayama 641-0012, Japan; and ¶Department of Biochemistry, Toho University, Chiba 274-8510, Japan

Edited by John E. Halver, University of Washington, Seattle, WA, and approved February 27, 2006 (received for review December 30, 2005)

We originally identified senescence marker protein 30 (SMP30) as a distinctive protein whose expression decreases in an androgen-independent manner with aging. Here, we report its sequence homology found in two kinds of bacterial gluconolactonases (GNLs) by using the BLAST search. Then, through a biochemical study, we identify SMP30 as the lactone-hydrolyzing enzyme GNL of animal species. SMP30 purified from the rat liver had lactonase activity toward various aldonolactones, such as D- and L-gluconono-δ-lactone, D- and L-gulono-γ-lactone, and D- and L-galactono-γ-lactone, with a requirement for Zn^{2+} or Mn^{2+} as a cofactor. Furthermore, in SMP30 knockout mice, no GNL activity was detectable in the liver. Thus, we conclude that SMP30 is a unique GNL in the liver. The lactonase reaction with L-gulono-γ-lactone is the penultimate step in L-ascorbic acid (AA) biosynthesis, and the essential role of SMP30 in this synthetic process was verified here by a nutritional study using SMP30 knockout mice. These knockout mice ($n = 6$), fed a vitamin C-deficient diet, did not thrive; i.e., they displayed symptoms of scurvy such as bone fracture and rachitic rosary and then died by 135 days after the start of receiving the deficient diet. The AA levels in their livers and kidneys at the time of death were <1.6% of those in WT control mice. In addition, by using the SMP30 knockout mouse, we demonstrate that the alternative pathway of AA synthesis involving D-glucurono-γ-lactone operates *in vivo*, although its flux is fairly small.

aging | osteogenic disorder | vitamin C

Senescence marker protein 30 (SMP30) is a 34-kDa protein whose tissue levels in the liver, kidney, and lung decrease with aging (1, 2). To examine the physiological function of SMP30, we established SMP30 knockout mice (3) and found that they were viable and fertile, although they were lower in body weight and shorter in life span than WT mice (4). Their livers were also far more susceptible to TNF-α- and Fas-mediated apoptosis than those of WT mice, indicating that SMP30 may act to protect cells from apoptosis (3). The livers of SMP30 knockout mice showed abnormal accumulations of triglycerides, cholesterol, and phospholipids (4). In addition, the lungs of these knockout mice had enlarged alveolar airspaces during their first to sixth month of life (2). However, the molecular mechanism of SMP30 function has remained obscure.

Recently, we reported that SMP30 acts as a hydrolase for diisopropyl phosphorofluoridate (5), a compound resembling chemical warfare nerve agents such as sarine, soman, and tabun. However, a physiological substrate for SMP30 must be present, because this compound is an artificial chemical. Our recent search for amino acid sequences resembling SMP30 was accomplished by using the BLAST program, which revealed that rat SMP30 is homologous with gluconolactonase (GNL) [EC 3.1.1.17], a lactone-hydrolyzing enzyme, of *Nostoc punctiforme* and *Zymomonas mobilis* (6). Therefore, we suspected that SMP30 is a GNL of animal species. In mammalian metabolism, GNL is involved in L-ascorbic acid (AA) biosynthesis, catalyzing the lactonization of L-gulonic acid, the reverse reaction of lactone hydrolysis (7). The product L-gulono-γ-lactone is oxidized to AA (8–10). In this study, to further investigate the identity of SMP30, we have unequivocally proven that it is a GNL. Purified rat liver SMP30 had GNL activity, as did a recombinant rat SMP30 produced in *Escherichia coli*. Furthermore, SMP30 knockout mice developed symptoms of scurvy when fed a vitamin C-deficient diet, verifying the pivotal role of SMP30 in AA biosynthesis.

Results

Identification of SMP30 as a GNL. Comparisons of the amino acid sequence of rat SMP30 by means of the BLAST program revealed that this protein was homologous with two kinds of bacterial GNLs. The total amino acid sequence of rat SMP30 (299 aa) shares 32% homology with that of *N. punctiforme* GNL (292 aa) (Fig. 1*A*), and a part of the amino acid sequence of rat SMP30 (222 aa, residues 9–230) shares 26% homology with that of *Z. mobilis* GNL (247 aa, residues 67–313) (Fig. 1*B*). Therefore, we speculated that the protein characterized previously as SMP30 in several animals is a GNL. For substantiation, we took this protein from the rat liver and purified it to apparent homogeneity as described in ref. 5. The elution profile of SMP30 obtained with Sephacryl S-200 HR chromatography, which was the final step of the purification process, coincided well with that of GNL activity (Fig. 7*A*, which is published as supporting information on the PNAS web site), clearly indicating an overlap between them. Conversely, GNL from the rat liver was purified to near homogeneity by a previously reported method (11). The resulting preparation gave a positive band on Western blot analysis by using anti-rat SMP30 antibody (Fig. 7*B*). Moreover, the main band of a gel processed by SDS/PAGE was subjected to sequence analysis after in-gel digestion with trypsin, and the amino acid sequence of its peptide (YFAGTMAEETAP) proved to be an exact match with an internal sequence (amino acid residues 113–124) of rat SMP30.

Expression of Catalytically Active Recombinant SMP30. The identity of SMP30 as a GNL was further confirmed by expressing a rat

Conflict of interest statement: No conflicts declared.

This paper was submitted directly (Track II) to the PNAS office.

Abbreviations: AA, L-ascorbic acid; BMD, bone mineral density; GNL, gluconolactonase; MBP, maltose-binding protein; SMP30, senescence marker protein 30.

‡Y.K., Y.I., and Y.S. contributed equally to this work.

‖To whom correspondence may be addressed. E-mail: nishikim@wakayama-med.ac.jp.

**To whom correspondence may be addressed at: Department of Molecular Pathology, Tokyo Metropolitan Institute of Gerontology, 35-2 Sakae-cho, Itabashi-ku, Tokyo 173-0015, Japan. E-mail: ishigami@tmig.or.jp.

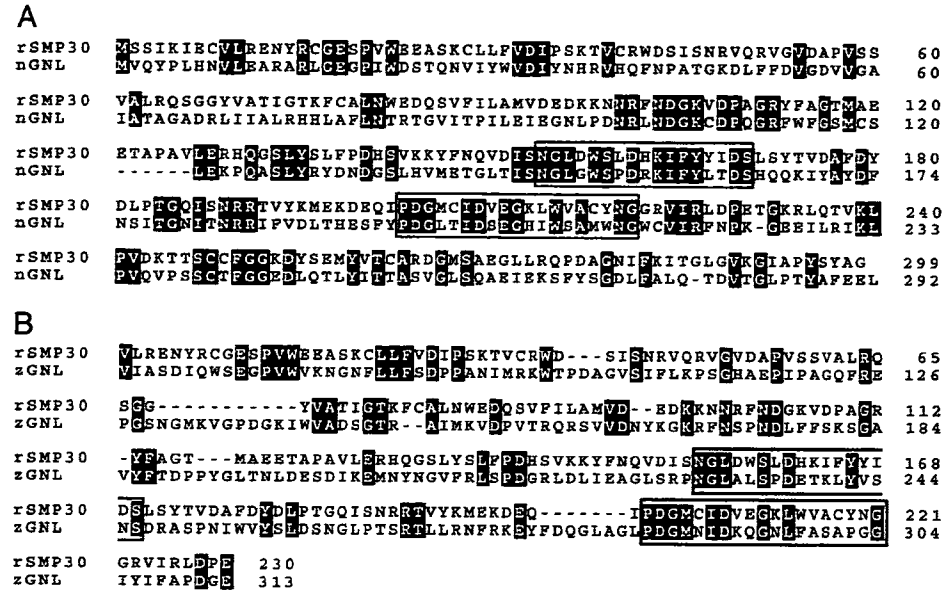

Fig. 1. Alignment of the amino acid sequences of rat SMP30 (rSMP30), *Nostoc* GNL (nGNL), and *Zymomonas* GNL (zGNL). (*A*) rSMP30 [National Center for Biotechnology Information (NCBI) accession no. CAA48786] vs. nGNL (NCBI accession no. ZP_00110023). (*B*) rSMP30 vs. zGNL (NCBI accession no. CAA47637). Two regions homologous among rat SMP30, nGNL, and zGNL are boxed in *A* and *B*.

SMP30 cDNA in *E. coli*. Recombinant SMP30 protein was expressed as a maltose-binding protein (MBP) fusion protein by using a chaperone coexpression system, and a soluble cell lysate was prepared. In this lysate, cells expressing the MBP–SMP30 fusion had clear-cut GNL activity (546 ± 18 nmol/min per mg of protein, mean ± SEM, $n = 3$) with D-glucono-δ-lactone used as a substrate, whereas the lysate of control cells (expressing a fusion of MBP with the α-fragment of β-gal) had no such activity. We further ascertained that the SMP30 fusion was the entity possessing GNL activity by subjecting this lysate containing the MBP–SMP30 fusion to native gel electrophoresis in triplicate and electroblotting onto a polyvinylidene fluoride membrane. The three parts of the membrane were respectively stained for GNL activity or immunochemically with anti-MBP or anti-SMP30 antibody. The bands stained in these three ways appeared at the same position (Fig. 2, lanes marked "2"). In contrast, a lysate of the cells expressing a fusion protein of MBP with the α-fragment of β-gal as a control did not contain any protein that was stained positive for GNL activity (Fig. 2 *A* and *C*, lane 1).

Enzymatic Characterization of SMP30. Subsequently, we measured GNL activity with a reaction mixture containing 10 mM D-glucono-δ-lactone, 75 μM $ZnCl_2$, and 0.42 μg/ml purified rat SMP30. The SMP30 hydrolyzed D-glucono-δ-lactone with a specific activity of 226 μmol/min per mg at an optimal pH of 6.4 with a linear increase up to an enzyme concentration of 0.42 μg of protein per ml (Fig. 8 *A* and *C*, which is published as supporting information on the PNAS web site). However, GNL activity was below the limit of detection in the absence of Zn^{2+}. Because a maximum level of GNL activity was observed at a Zn^{2+} concentration of 75 μM (Fig. 8*B*), this amount of Zn^{2+} was used in all experiments for enzymatic characterization.

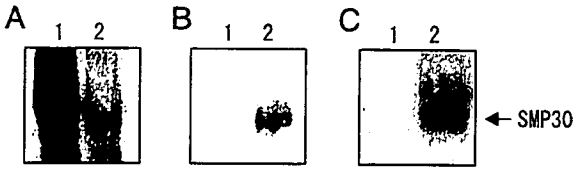

Fig. 2. Immunoblot analysis after native PAGE and activity staining of recombinant rat SMP30. Samples were electrophoresed on a native polyacrylamide gel, and the proteins on the gel were electroblotted onto a membrane. Detection of specific proteins was carried out with anti-MBP antibody (*A*), anti-rat SMP30 antibody (*B*), and activity staining (*C*). To stain for enzyme activity, D-galactono-γ-lactone was used as substrate. Lane 1, the lysate of *E. coli* cells expressing a fusion of MBP with β-gal α-fragment (control); lane 2, the lysate of *E. coli* cells expressing a fusion of MBP with rat SMP30. The arrow shows the position of a fusion of MBP with rat SMP30.

Other divalent metal ions were also tested at a concentration of 75 μM in the standard assay mixture. Only Mn^{2+} ions were effective, giving 27% of the enzyme activity observed with Zn^{2+} (Fig. 8*B*), whereas Mg^{2+}, Co^{2+}, Ca^{2+}, and Cd^{2+} ions gave no activity. However, slight enzyme activity ($\ll$10%) was observed with 3 mM concentrations of these metal ions and a 10-fold higher concentration of SMP30 (4.2 μg/ml) (data not shown).

Next, we studied the kinetics of the GNL reaction. Hyperbolic kinetics were normal (Fig. 9, which is published as supporting information on the PNAS web site), and a Lineweaver–Burk plot of the data yielded an apparent K_m value of 9.4 mM and a V_{max} value of 345 μmol/min per mg (Fig. 9 *Inset*). The lactonase activities for a variety of sugar lactones by SMP30 are summarized in Table 2, which is published as supporting information on the PNAS web site. D-glucono-δ-lactone was the best substrate. SMP30 also hydrolyzed L-glucono-δ-lactone, D-gulono-γ-lactone, L-gulono-γ-lactone, D-galactono-γ-lactone, and L-galactono-γ-lactone, indicating that SMP30 has broad substrate specificity for aldonolactones. D-aldonolactones were better substrates than the corresponding enantiomers. SMP30 had no detectable hydrolyzing activity toward D-ribono-γ-lactone, D-mannono-γ-lactone, or D-glucoheptono-γ-lactone.

An Essential Role of SMP30 in AA Biosynthesis. To examine whether these substrates are attacked only by SMP30 in the rat liver, we compared lactonase activity in livers from SMP30Y$^-$ and SMP30Y$^+$ mice. Liver extracts from SMP30Y$^+$ mice hydrolyzed D-glucono-δ-lactone, D-gulono-γ-lactone, and D-galactono-γ-lactone, whereas those from SMP30Y$^-$ mice had no detectable

Table 1. Absence of GNL activity in livers from SMP30 knockout mice

Substrate	Specific activity, μmol/min per mg	
	SMP30Y+	SMP30Y−
D-glucono-δ-lactone	9.0 ± 0.6	ND
D-gulono-γ-lactone	0.5 ± 0.1	ND
D-galactono-γ-lactone	0.4 ± 0.1	ND

The hydrolytic activities for the substrates of SMP30 were determined by the method described in *Materials and Methods*. The values are the average ± SEM for livers from five animals. ND, no detectable enzyme activity.

hydrolyzing activity toward these lactones (Table 1). Clearly, therefore, SMP30 is a unique enzyme that effectively hydrolyzes various aldonolactones in the liver. Because the lactonization of L-gulonic acid to L-gulono-γ-lactone, the reverse reaction of the lactonase reaction, is the penultimate step of AA synthesis, we investigated the role of SMP30 in this metabolic process by using SMP30 knockout mice. Ten days after weaning at the age of 30 days, SMP30Y− and SMP30Y+ mice, six each, were fed a vitamin C-deficient diet. One of the knockout mice started to lose weight after 25 days of consuming this diet (at an age of 65 days), walked with an abnormal gait after 31 days, and died after 37 days. The average body weight of the other five knockout mice started to decrease after 56 days of the vitamin C-deficient diet (at an age of 96 days) (Fig. 3*A*); their gait became abnormal at that time, and they died by the 106th to 135th days of this dietary deficiency. The AA level in plasma of SMP30Y− mice after 106 days of consuming the deficient diet was <1% of that in SMP30Y+ mice (Fig. 3*B*). The livers and kidneys of SMP30Y− mice at the time of death contained <1.6% of the AA levels in the SMP30Y+ mice (Fig. 3 *C* and *D*).

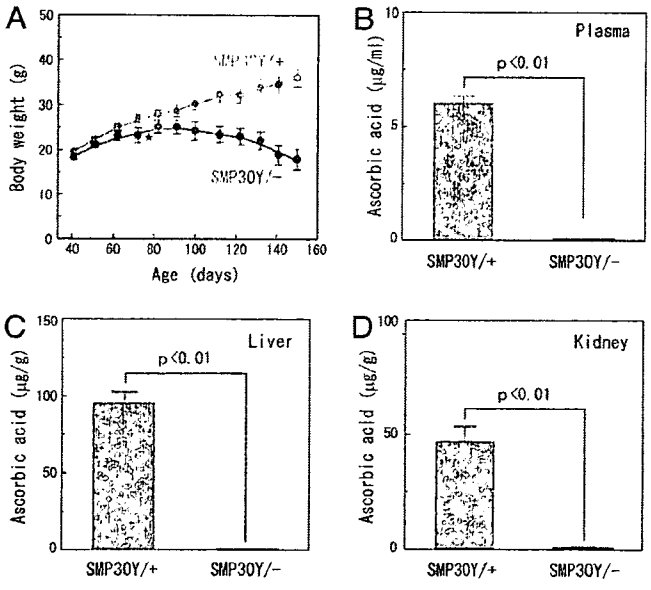

Fig. 3. Body weight changes and AA levels in the plasma, livers, and kidneys of SMP30Y− and SMP30Y+ mice. SMP30Y− and SMP30Y+ mice, six each, were weaned at 30 days of age and fed autoclaved mouse chow (containing ≈55 mg of AA per kg) for 10 days; then, they were fed a vitamin C-deficient diet until all SMP30Y− animals were dead. (*A*) Body weight changes of SMP30Y− (pink circles) and SMP30Y+ (green circles) mice. One SMP30Y− mouse died after 37 days (indicated by star), and the others died after 106–135 days of consuming the vitamin C-deficient diet. (*B–D*) Blood was taken from all tested animals (six WT and five knockout mice) after 106 days of this diet, and AA levels in the plasma (*B*) were measured. All mice were killed after 136 days of receiving the deficient diet, and AA levels in the liver (*C*) and kidney (*D*) were measured. Except for blood, all specimens of SMP30Y− mice were taken after death. Values are expressed as mean ± SEM of five or six animals.

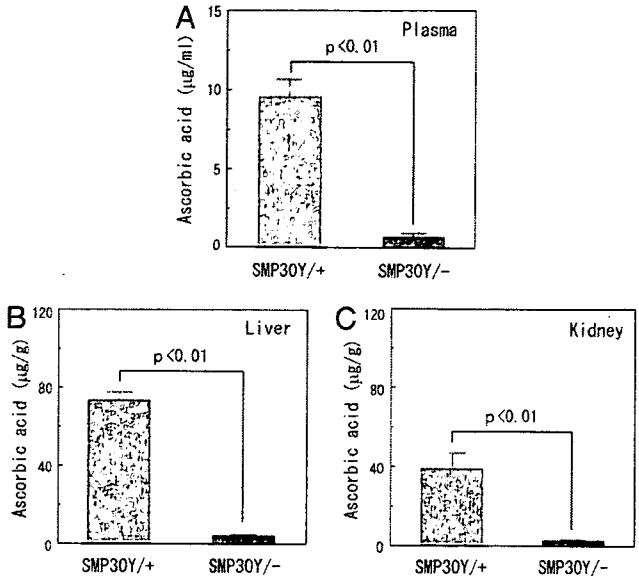

Fig. 4. AA levels in the plasma, livers, and kidneys from SMP30Y− and SMP30Y+ mice that were fed autoclaved mouse chow. SMP30Y− and SMP30Y+ mice, four each, were weaned at 30 days of age and fed autoclaved mouse chow (containing ≈55 mg of AA per kg) for 80 days (age 110 days). AA levels were then measured in their plasma (*A*), livers (*B*), and kidneys (*C*). Values are expressed as mean ± SEM of four animals.

For the previous studies, our SMP30Y− mice were fed autoclaved mouse chow after weaning, and this food contains ≈55 mg/kg of vitamin C. When we assessed the vitamin C status of such mice after 80 days of eating autoclaved chows, their plasma, livers, and kidneys contained only 6–8% of the AA values in the WT mice (Fig. 4). Thus, the knockout mice that were fed autoclaved mouse chow proved to be severely vitamin C-deficient.

Osteogenic Disorder of SMP30 Knockout Mice. Because thin, brittle bones with a tendency to fracture are known as characteristic manifestations of scurvy, we checked the skeletal structure of SMP30Y− and SMP30Y+ mice by x-ray examination after they had consumed the vitamin C-deficient diet for 59 days (at an age of 99 days) (Fig. 5 *A* and *B*). Fracture at the distal end of their femurs (Fig. 5*B Inset*) and rachitic rosaries at the junction of costae and costal cartilages (Fig. 5*B*) were prominent in a SMP30Y− mouse (Fig. 5*D*), but not a SMP30Y+ mouse (Fig. 5*C*). Moreover, subcranial total bone mineral density (BMD) and body fat were significantly decreased in SMP30Y− mice compared with SMP30Y+ mice (Fig. 5 *E* and *F*).

Occurrence of an Alternative Pathway of AA Synthesis. Two pathways were proposed as forming the last part of the AA synthetic pathway (12). Obviously, the main pathway of this process dealt with here includes the steps from D-glucose to L-gulonic acid (detailed on the left side of Fig. 6*A*). However, for the formation of L-gulono-γ-lactone, the immediate precursor to AA, another pathway branches from D-glucuronic acid (Fig. 6*A*, right side). To clarify whether the latter pathway exists in the mammalian metabolism, we injected D-glucurono-γ-lactone i.p. into SMP30Y− mice and measured the amount of AA excreted in their urine. We used the lactone for delivery of D-glucuronic acid

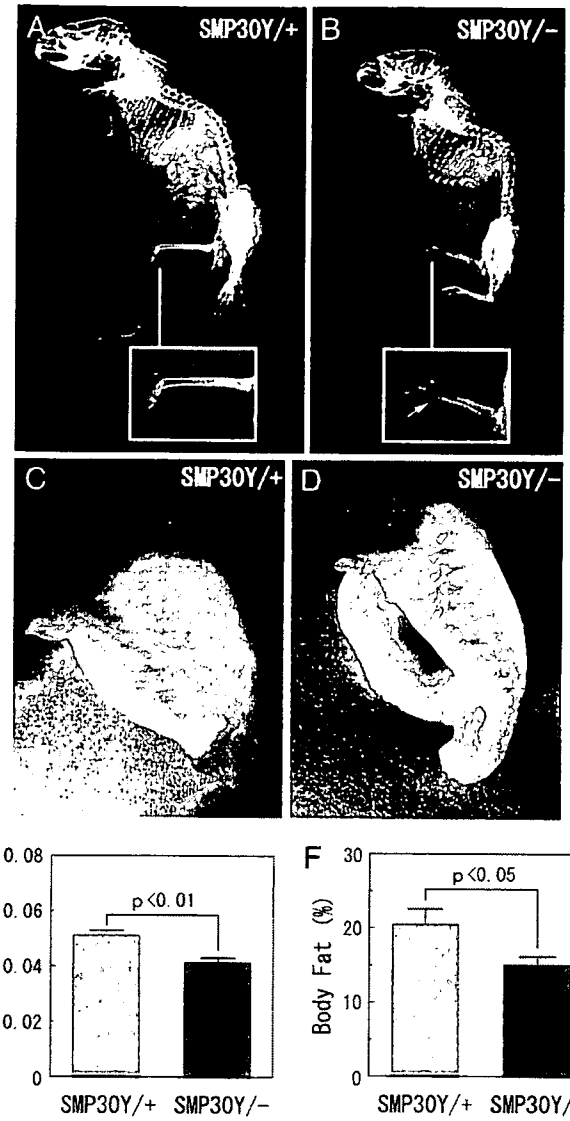

Fig. 5. Osteogenic disorder of SMP30 knockout mice. SMP30Y$^-$ and SMP30Y$^+$ mice at an age of 40 days were fed a vitamin C-deficient diet for 59 days (animals' age was 99 days). (*A–D*) X-ray images show the skeletal structures of SMP30Y$^+$ (*A*) and SMP30Y$^-$ (*B*) mice. *Insets* show enlargements of the femoral region; an arrow points to the distal femur fracture of a SMP30 knockout mouse. A rachitic rosary of the SMP30Y$^-$ mouse observed after evisceration (*D*) is compared with that area in a control mouse (*C*). Arrowheads in *B* and *D* indicate a rachitic rosary at the junction of costae and costal cartilage. (*E* and *F*) Subcranial total BMD (*E*) and body fat percentage (*F*) of SMP30Y$^-$ and SMP30Y$^+$ mice were determined by PIXImus2 densitometry as described in *Materials and Methods*. Values are expressed as mean ± SEM of five or six animals.

into liver cells, where AA synthesis occurs, because the lactone would be more easily incorporated into the cells than D-glucuronic acid and would come into equilibrium with this acid by catalysis of uronolactonase (12, 13). As a result, the excretion of AA was appreciably increased by the injection, albeit in a small amount, whereas AA excretion was not affected by the saline injected as a control (Fig. 6*B*). Thus, the alternative pathway was clearly operational here, regardless of its small flux.

Discussion

This study provides unequivocal evidence that SMP30 is the bona fide GNL in the AA biosynthetic pathway of mammals. In

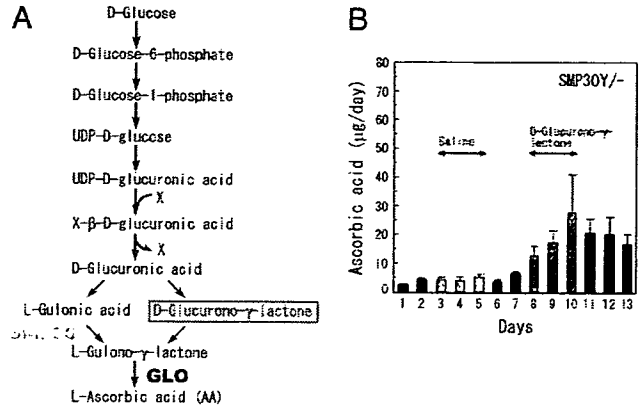

Fig. 6. Increased excretion of AA in the urine after administration of D-glucurono-γ-lactone. (*A*) The pathway of AA biosynthesis. The pathway from D-glucose to L-gulonic acid is shared with that of early steps in the uronic acid cycle. X is a conjugating molecule for glucuronidation. GLO, L-gulono-γ-lactone oxidase. (*B*) SMP30Y$^-$ mice were fed autoclaved mouse chow for 60 days after weaning and were housed individually in metabolic cages starting on day 1. Saline was injected i.p. from day 3 to day 5; then, D-glucurono-γ-lactone (0.7 mg/g of body weight) dissolved in saline was injected i.p. from day 8 to day 10. Urine samples were collected, and their AA concentrations were measured. Values are expressed as mean ± SEM of four SMP30Y$^-$ mice.

support, (*i*) SMP30 purified from the rat liver exhibited GNL activity (Fig. 7 and Table 2), (*ii*) a partial amino acid sequence of GNL purified from rat liver was identical to that of the reported sequence of rat SMP30, and (*iii*) the GNL was recognized by antibody directed to rat SMP30. Moreover, recombinant rat SMP30 expressed in *E. coli* showed GNL activity (Fig. 2). Overall, the purified SMP30 had the same substrate specificity toward multiple lactones as previously reported for GNL (7, 11, 13, 14). With respect to the requirement for metal in this process, Zn^{2+} and Mn^{2+} were both effective activators, although it was previously reported that Mn^{2+} was dominantly effective but that Zn^{2+} had no effect. This discrepancy is possibly due to differing experimental settings (11, 13, 14).

Measurements of GNL activity disclosed that the liver extract of SMP30 knockout mice lacked any such activity under conditions in which the WT extract was markedly active for three known substrates of GNL (Table 1). This outcome indicates that SMP30 is the unique lactone-hydrolyzing enzyme for these substrates in the liver. An essential role of SMP30 in AA biosynthesis in mice was evidenced by a nutritional study using SMP30 knockout mice. AA is produced from the ultimate hexose precursor D-glucose, and, in this pathway, L-gulonic acid, an intermediary metabolite of the uronic acid cycle, is lactonized to form L-gulono-γ-lactone, which in turn is oxidized to AA (Fig. 6*A*). GNL is known to catalyze the former reaction (8–10). In our experiments, scurvy developed in SMP30 knockout mice that were fed a vitamin C-deficient diet (Figs. 3 and 4). Their symptoms of scurvy included bone fractures, rachitic rosaries, and premature death by 135 days after institution of the vitamin C-deficient diet. In view of this fact, one can understand the phenotypes of SMP30 knockout mice mentioned in the Introduction (abnormally low body weight, shortened life span, susceptibility to hepatic apoptosis, etc., compared with WT mice). For our previous studies (2–4), these mice were fed autoclaved mouse chow, which we now know contains too little vitamin C to maintain normal levels of AA in tissues (Fig. 4). Accumulations of triglycerides, phospholipids, and cholesterol in the livers of these knockout mice may be associated with impaired fatty acid oxidation, probably because of decreased synthesis of carnitine, which plays a role in the transport of

long-chain fatty acids into mitochondria. AA is required as a cofactor in two hydroxylation reactions in carnitine biosynthesis (15). In fact, AA-deficient guinea pigs were shown to have abnormalities of lipid metabolism, such as hyperlipidemia and hypercholesterolemia (16). Another clinical feature of young SMP30 knockout mice is enlargement of alveolar airspaces compared with those of WT mice (2). A similar change was reported in ODS (osteogenic disorder Shionogi) rats that survived for a long time on a vitamin C-deficient diet (17). However, never before did we observe scurvy symptoms in the knockout mice that were fed autoclaved mouse chow, despite their smaller body size and shorter life span (3, 4). Assuming that an average weight of mice is 25 g and that the amount of chow taken per day is 4 g (18), SMP30 knockout mice ingest <0.01 mg/g of body weight per day. Based on the observation that 0.02 mg/g of body weight per day cannot sustain normal body function in a scurvy-prone mouse whose L-gulono-γ-lactone oxidase gene was deleted (19), the SMP30 knockout mice seem not to have ingested enough vitamin C. Probably, a small amount of AA may be synthesized through the alternative pathway (Fig. 6*A*) previously proposed based on an enzymatic study (20) and demonstrated here in SMP30 knockout mice. Furthermore, the absence of GNL may lead to decreased degradation of AA, because GNL can hydrolyze the lactone ring of dehydroascorbic acid, the oxidation product of AA, to 2,3-dioxo-L-gulonic acid, as formerly reported (20).

Because SMP30 is abundant in the kidney and also present, although in lesser amounts, in other organs (21), this protein must have some function other than AA synthesis, which does not occur at all these sites. SMP30 may prevent the production of glycated proteins by hydrolyzing D-glucono-δ-lactone. It is possible that this lactone is formed from D-glucose by glucose dehydrogenase *in vivo*, and it may be involved in glycation of proteins. In fact, human and rat hemoglobin was shown to be glycated with D-glucono-δ-lactone (22). Glycated proteins, especially advanced glycation end products, are known to cause the deterioration of cellular functions; therefore, SMP30 may protect cells from such an effect.

Materials and Methods

Chemicals. L-glucono-δ-lactone, D-gulono-γ-lactone, L-gulono-γ-lactone, L-galactono-γ-lactone, D-ribono-γ-lactone, D-glucoheptono-γ-lactone, and D-mannono-γ-lactone were purchased from Sigma-Aldrich. D-glucono-δ-lactone, D-galactono-γ-lactone, and other reagents were purchased from Wako Pure Chemical (Osaka).

Animals. Male Wister rats, 3–9 months of age, were obtained from the Animal Facility at Tokyo Metropolitan Institute of Gerontology, and their livers were used as a source of purified SMP30. For purification of GNL, 10-week-old male Wister rats purchased from Kiwa Laboratory Animals (Misato-cho, Japan) were used. SMP30 knockout mice were previously generated with the gene-targeting technique (3), and heterozygous female mice ($SMP30^{+/-}$) were mated with male knockout mice ($SMP30Y^{-}$) to produce knockout and WT ($SMP30Y^{+}$) littermates. These littermates were fed autoclaved mouse chow (CRF-1; Charles River Breeding Laboratories) ad libitum with free access to water and used for measurement of GNL activity in the liver when the animals were 6 months old. The autoclaved chow contained ≈55 mg of AA per kg as determined at the time of experimentation.

In a nutritional study, $SMP30Y^{-}$ and $SMP30Y^{+}$ mice were weaned at 30 days of age and fed autoclaved mouse chow for 10 days, followed by a vitamin C-deficient diet (CL-2; CLEA Japan, Tokyo). Throughout the experiments, animals were maintained on 12-h light/dark cycles in a controlled environment. All experimental procedures using laboratory animals were approved by the Animal Care and Use Committee of Tokyo Metropolitan Institute of Gerontology.

Purification of SMP30 from Rat Liver. SMP30 was purified from a soluble fraction of rat livers as described in ref. 5. Briefly, liver homogenate was fractionated by ammonium sulfate precipitation followed by a successive series of chromatographies on DEAE-Sephacel, Phenyl Sepharose CL-4B, and Sephacryl S-200 HR columns (all from Amersham Pharmacia Biosciences). The elution of SMP30 was followed by the dot-blot immunoassay described in ref. 5. The purified SMP30 was stored at −70°C until use.

Purification of GNL and Sequence Analysis of Its Peptide. GNL was purified from rat livers according to the method of Grossman and Axelrod (11), with slight modifications. Briefly, a soluble fraction of the liver homogenate was heated at 50°C for 30 min, and the resulting soluble fraction was fractionated with ammonium sulfate. The fraction with GNL activity was further purified by successive chromatographies on columns of Sephadex G-150 (Amersham Pharmacia Fine Chemicals), Resource Q (Amersham Pharmacia Biosciences), and Bio-Gel HTP (Bio-Rad). After the final preparation was subjected to SDS/PAGE, the main band was excised, and the protein in the gel was digested with trypsin. One of the peptides produced was sequenced through the custom service of APRO Life Science Institute (Naruto, Japan).

GNL and Related Activities. GNL activity was measured by the change in absorbance of the pH indicator *p*-nitrophenol caused by free acid formation from the lactone (23). The standard mixture contained 10 mM D-glucono-δ-lactone, 10 mM Pipes (pH 6.4), 0.25 mM *p*-nitrophenol, 75 μM $ZnCl_2$, and an enzyme in a total volume of 1 ml. The substrate solution was freshly prepared immediately before the assay. The reaction was followed by monitoring a decrease in absorbance at 405 nm, and the acid production rate was determined with a calibration curve obtained by using known amounts of HCl. The rate of spontaneous hydrolysis of the lactone was subtracted from the total rate. To assess whether a divalent metal ion was required for GNL activity, we tested $ZnCl_2$, $MnCl_2$, $MgCl_2$, $CoCl_2$, $CaCl_2$, and $CdCl_2$ in this regard and then determined the hydrolyzing activity for other lactones with the same procedure, except for the substrate.

Lactonase activity was then analyzed in livers removed from mice and homogenized with ice-cold homogenization buffer (10 mM Tris·HCl, pH 8.0/1 mM phenyl methanesulfonyl fluoride) for 30 s at high speed with a Polytron homogenizer. The homogenate was centrifuged at 10,000 × *g* for 10 min. The protein concentration of the sample was determined by BCA protein assay (Pierce) using BSA as a standard. The lactone-hydrolyzing activity was assayed by using various lactones under the standard conditions described above. In the purification of rat GNL, lactonase activity was measured by recording pH change with a pH meter, essentially as described in ref. 24.

Expression of Recombinant Rat SMP30. Total RNA was prepared from a rat liver and used to produce a single-strand cDNA with SuperScript II RNase H^{-} reverse transcriptase (Life Technologies, Rockville, MD) following the manufacturer's protocol. A SMP30 cDNA was amplified by PCR from this cDNA such that an EcoRI site would be produced at the both ends of the product. The PCR was carried out by using *PfuUltra* DNA polymerase (Stratagene) with a sense primer (5′-GAATTCATGTCTTC-CATCAAGATTG-3′) and an antisense primer (5′-GAATTCT-TACCCTGCATAGGAATATG-3′). The amplified DNA was digested with EcoRI and inserted into the EcoRI site of the *E. coli* expression vector pMAL-c2x (New England Biolabs). The

constructed plasmid pMAL-c2x-rSMP30 was used to transform *E. coli* BL21 that had previously been transformed with pGro7 (Takara Bio, Tokyo) for expression of two chaperone proteins: GroEL and GroES. The resulting clone was used to express rat SMP30 as a fusion protein with MBP as follows. It was cultured at 37°C overnight in LB containing 0.2% glucose, 100 μg/ml ampicillin, and 20 μg/ml chloramphenicol. After the cell suspension was diluted 100-fold with the same culture medium, D-arabinose (4 mg/ml) was added for expression of the chaperone proteins and cultured for 1.6 h at 37°C. Then, the expression of MBP–SMP30 fusion protein was induced by adding isopropyl β-D-thiogalactoside to a final concentration of 0.3 mM and culturing for 3 h at 30°C. For control experiments, pMAL-c2x was used instead of pMAL-c2x-rSMP30, and a fusion protein of MBP with the α-fragment of β-gal was induced in the same way as above. The cells were washed with Dulbecco's phosphate buffered saline, resuspended in 20 mM Tris·HCl buffer (pH 7.4) containing 200 mM NaCl, and stored at −30°C until use.

Activity Staining and Western Blotting for Recombinant MBP–SMP30 Fusion Protein. Suspensions of the test and control cells were sonicated and centrifuged at 9,000 × *g* for 30 min at 4°C. Each resulting supernatant (60 μg of protein) was electrophoresed on a 7% polyacrylamide gel by the method of Davis (25), with some modifications. Proteins in the gel were transferred onto a polyvinylidene fluoride membrane with 25 mM Tris/192 mM glycine as a transfer buffer. Subsequent staining for GNL activity involved immersing the membrane successively in 5 mM Tris·HCl buffer (pH 6.8) containing 1 mM DTT and 1 mM $MnCl_2$ (buffer A), then in a mixture of buffer A and 0.04% methyl red in 60% ethanol (9:1), and finally in buffer A containing 80 mM D-galactono-γ-lactone until the red color appeared.

For Western blotting, the supernatant (20 μg of protein) was electrophoresed in duplicate, and proteins were transferred onto a polyvinylidene fluoride membrane in the same way. The membrane was blocked overnight with a mixture of 2% BSA and 7% skim milk and cut into halves. One half was incubated with anti-MBP rabbit antibody (1:3,000 dilution; New England Biolabs), and the other half was incubated with anti-rat SMP30 rabbit antibody (1:3,000 dilution; Cosmo Bio, Tokyo) (3). Then, both half-membranes were incubated with horseradish peroxidase-conjugated anti-rabbit IgG antibody (1:5,000 dilution; Cappel). MBP and SMP30 were visualized with an ECL (enhanced chemiluminescence) detection kit (Amersham Pharmacia Biosciences).

Measurement of AA. Plasma was mixed with nine volumes of 20% metaphosphate containing 1% $SnCl_2$, and the mixture was centrifuged at 10,000 × *g* for 10 min at 4°C. Livers and kidneys were homogenized in 14 volumes of 5.4% metaphosphate, and the homogenate was centrifuged as above. For measurement of AA excreted into urine, a mouse was housed in a metabolic cage, and urine was collected in a bottle with 10% metaphosphate for 24 h. The amount of 10% metaphosphate had been adjusted to keep its concentration >5% after dilution with urine. The volume of the urine–metaphosphate mixture was recorded, and the mixture was centrifuged as above. All samples obtained after centrifugation were kept at −80°C until use. AA in samples was derivatized with dinitrophenylhydrazine and analyzed by HPLC with a Shodex-5SIL-4E column (4.6 × 250 mm; Showa Denko, Tokyo). The mobile phase was hexane/ethylacetate/acetic acid (5:4:1) at a flow rate of 1 ml/min, and the absorbance at 495 nm was recorded (26, 27). AA in mouse chow was determined by the same method after extraction into 15% metaphosphate.

Quantification of BMD and Body Fat Percentage. Subcranial total BMD and body fat percentage were determined by densitometry with the PIXImus2 imager (General Electric/Lunar, Madison, WI). Field calibration and calibration vs. the quality-control phantom were performed each day before imaging. Each mouse was positioned reproducibly in a prone position on the imaging tray and scanned three times. The coefficients of variance for BMD and body fat percentage were 0.9% and 2.2%, respectively, for *in vitro* measurements.

Statistical Analysis. The results are expressed as mean ± SEM. The probability of statistical differences between experimental groups was determined by Student's *t* test or ANOVA as appropriate. One and two-way ANOVAs were performed by using KALEIDAGRAPH software (Synergy Software, Reading, PA).

We thank Ms. P. Minick for excellent assistance in the review of English and Mr. H. Hosoi and Ms. Y. Takenaka for participation in the purification of GNL in the training course on basic medicine at Wakayama Medical University. This work was supported by a Grant-in-Aid for Scientific Research (to S.H. and S.K.) and a Grant-in-Aid for Young Scientists (B) (to Y.I.) from the Japanese Ministry of Education, Culture, Sports, Science, and Technology and grants from Health Science Research Grants for Comprehensive Research on Aging and Health supported by the Ministry of Health, Labor, and Welfare of Japan (to A.I.), the Smoking Science Foundation (to N.M.), and the Vitamin C Research Committee of Japan (to M.N.).

1. Fujita, T., Uchida, K. & Maruyama, N. (1992) *Biochim. Biophys. Acta* **1116**, 122–128.
2. Mori, T., Ishigami, A., Seyama, K., Onai, R., Kubo, S., Shimizu, K., Maruyama, N. & Fukuchi, Y. (2004) *Pathol. Int.* **54**, 167–173.
3. Ishigami, A., Fujita, T., Handa, S., Shirasawa, T., Koseki, H., Kitamura, T., Enomoto, N., Sato, N., Shimosawa, T. & Maruyama, N. (2002) *Am. J. Pathol.* **161**, 1273–1281.
4. Ishigami, A., Kondo, Y., Nanba, R., Ohsawa, T., Handa, S., Kubo, S., Akita, M. & Maruyama, N. (2004) *Biochem. Biophys. Res. Commun.* **315**, 575–580.
5. Kondo, Y., Ishigami, A., Kubo, S., Handa, S., Gomi, K., Hirokawa, K., Kajiyama, N., Chiba, T., Shimokado, K. & Maruyama, N. (2004) *FEBS Lett.* **570**, 57–62.
6. Kanagasundaram, V. & Scopes, R. (1992) *Biochim. Biophys. Acta* **1171**, 198–200.
7. Bublitz, C. & Lehninger, A. L. (1961) *Biochim. Biophys. Acta* **47**, 288–297.
8. Burns, J. J. (1960) in *Metabolic Pathway*, ed. Greenberg, D. M. (Academic, New York), Vol. 1, pp. 341–356.
9. Nishikimi, M. & Yagi, K. (1996) in *Subcellular Biochemistry–Ascorbic Acid: Biochemistry and Biomedical Cell Biology*, ed. Harris, J. R. (Plenum, New York), Vol. 25, pp. 17–39.
10. Nishikimi, M., Okamura, M. & Ohta, Y. (2003) in *Recent Research Developments in Biophysics and Biochemistry*, ed. Pandalai, S. G. (Research Signpost, Kerala, India), Vol. 3, Part 1, pp. 531–545.
11. Grossman, S. H. & Axelrod, B. (1973) *J. Biol. Chem.* **248**, 4846–4851.
12. Shimazono, N. & Mano, Y. (1961) *Ann. N.Y. Acad. Sci.* **92**, 91–104.
13. Winkelman, J. & Lehninger, A. L. (1958) *J. Biol. Chem.* **233**, 794–799.
14. Kawada, M., Takiguchi, H., Kagawa, Y., Suzuki, K. & Shimazono, N. (1962) *J. Biochem. (Tokyo)* **51**, 405–415.
15. Rebouche, C. J. (1991) *Am. J. Clin. Nutr.* **54**, 1147S–1152S.
16. Ha, T. Y., Otsuka, M. & Arakawa, N. (1990) *J. Nutr. Sci. Vitaminol. (Tokyo)* **36**, 227–234.
17. Kono, K., Asai, K., Kuzuya, F. & Harada, T. (1990) in *Vitamin C and the Scurvy-Prone ODS Rat*, eds. Fujita, T., Fukase, M. & Konishi, T. (Elsevier, Amsterdam), pp. 147–155.
18. Bernstein, S. E. (1966) in *Biology of the Laboratory Mouse*, ed. Green, E. L. (Dover, New York), 2nd Ed., pp. 337–350.
19. Maeda, N., Hagihara, H., Nakata, Y., Hiller, S., Wilder, J. & Reddick, R. (2000) *Proc. Natl. Acad. Sci. USA* **97**, 841–846.
20. Kagawa, Y. & Takiguchi, H. (1962) *J. Biochem. (Tokyo)* **51**, 197–203.
21. Fujita, T., Shirasawa, T., Uchida, K. & Maruyama, N. (1992) *Biochim. Biophys. Acta* **1132**, 297–305.
22. Lindsay, R. M., Smith, W., Lee, W. K., Dominiczak, M. H. & Baird, J. D. (1997) *Clin. Chim. Acta* **263**, 239–247.
23. Hucho, F. & Wallenfels, K. (1972) *Biochim. Biophys. Acta* **276**, 176–179.
24. Nishikimi, M., Koshizaka, T., Mochizuki, H., Iwata, H., Makino, S., Hayashi, Y., Ozawa, T. & Yagi, K. (1988) *Biochem. Int.* **16**, 615–621.
25. Davis, B. J. (1964) *Ann. N.Y. Acad. Sci.* **121**, 404–427.
26. Kishida, E., Nishimoto, Y. & Kojo, S. (1992) *Anal. Chem.* **64**, 1505–1507.
27. Kodaka, K., Inagaki, S., Ujie, T., Ueno, T. & Suda, H. (1985) *Vitamin* **59**, 451–455.

Available online at www.sciencedirect.com
SCIENCE DIRECT
Mechanisms of Ageing and Development 127 (2006) 451–457
mechanisms of ageing and development
www.elsevier.com/locate/mechagedev

SMP30 deficiency causes increased oxidative stress in brain

Tae Gen Son [a], Yani Zou [a], Kyung Jin Jung [a], Byung Pal Yu [b], Akihito Ishigami [c], Naoki Maruyama [c], Jaewon Lee [a,*]

[a] *Department of Pharmacy, College of Pharmacy and Research Institute for Drug Development, Longevity Life Science and Technology Institutes, Pusan National University, Geumjeong-gu, Busan 609-735, South Korea*
[b] *The University of Texas Health Science Center, San Antonio, TX 78229-390, USA*
[c] *Department of Molecular Pathology, Tokyo Metropolitan Institute of Gerontology, Tokyo 173-0015, Japan*

Accepted 11 January 2006
Available online 28 February 2006

Abstract

Senescence marker protein 30 (SMP30), an important aging marker molecule, has been identified functionally as a calcium regulatory protein. Recent evidence showed its new assumed role as an effective anti-oxidative property. However, the role of SMP30 in the brain has not been explored. To delineate its role in the brain, we utilized SMP30 knock-out (SMP30 KO) mice in the current study. We focused on the oxidative status of the brain by examining selected oxidative markers in brains of SMP30 KO mice. Results showed that the generation of reactive species (RS) and NADPH oxidase activities were significantly elevated in SMP30 deficient brain. The increased oxidative status in these mice was further confirmed by increased oxidatively modified proteins such as dityrosine formation and carbonylation in the cortex of SMP30 KO mice. Moreover, SMP30 deficient brain showed the increased Mac-1 protein and myeloperoxidase (MPO) activity in the brain, supporting the putative anti-oxidative action of SMP30. Interestingly, the activities of major antioxidant enzymes, superoxide dismutase, catalase and reduced glutathione peroxidase in the brain were not affected by SMP30 depletion. Our results documented that brain SMP30 has a protective action against oxidative damage, without influencing antioxidant enzyme status.

Keywords: SMP30; Oxidative stress; Dityrosine; Carbonylation; Myelopeoxidase

1. Introduction

SMP30 was discovered by Fujita who identified it as a senesence marker molecule that decreases an androgen-independently with aging (Fujita et al., 1992). SMP30 was later recognized to poses a Ca^{2+} binding capacity, for which named as regucalcin (Fujita et al., 1999).

Many recent evidences show that SMP30 has been demonstrated to play multifunctional roles as a regulatory protein in intracellular signaling processes, such as activation of Akt on apoptosis (Matsuyama et al., 2004) and the regulation of various Ca^{2+}-dependent protein kinase and tyrosine kinase, protein phosphatases, nitric oxide (NO) synthase, and suppression of nuclear DNA and RNA syntheses (Izumi et al., 2003; Izumi and Yamaguchi, 2004).

The recently developed SMP30 knock-out (KO) mice have provided us the experimental paradigm to analyze the critical roles of SMP30. SMP30 KO mice were generated by disruption of the third exon of SMP30 gene on the X chromosome (Ishigami et al., 2002). Although these mice show about 20% lower in body weight and a shorter life span compared to the wild type (WT), they are fertile and apparently healthy (Maruyama et al., 2004). Many of the phenotypic changes mimic the premature aging processes. For example, SMP30 KO mice showed hepatic lipid droplets, abnormally enlarged mitochondria with indistinct cristae, and enlarged lysosomes (Ishigami et al., 2004). Likewise, deposition of lipofuscin as an aging marker in renal tubular epithelial cells was found in the kidney of SMP30 KO mice (Maruyama et al., 2004). Moreover, SMP30 KO mice have an increased susceptibility to apoptosis induced by TNF-α, Fas ligand, and calcium ionophore in hepatocytes (Ishigami et al., 2002).

Other reports indicate that SMP30 participates in controlling the antioxidant enzyme activity. SMP30 has an

* Corresponding author. Tel.: +82 51 510 2805; fax: +82 51 513 6754.
E-mail address: neuron@pusan.ac.kr (J. Lee).

0047-6374/$ – see front matter © 2006 Elsevier Ireland Ltd. All rights reserved.
doi:10.1016/j.mad.2006.01.005

activating effect on superoxide dismutase (SOD) in liver (Fukaya and Yamaguchi, 2004) and heart cytosol (Ichikawa and Yamaguchi, 2004) of SMP30 transgenic mice. It has been suggested that the age-associated decrease of SMP30 is closely associated with oxidative stress. For instance, treatment of carbon tetrachloride as acute oxidative stress markedly suppresses the SMP30 expression in liver (Ishigami et al., 2001). In addition, SMP30 suppresses the generation of reactive species (RS) in hepatocytes (Feng et al., 2004), and decreased levels of SMP30 in aging process were correlated with the increased levels of RS generation in rat liver and kidney (Jung et al., 2004). It has also been reported that a significant reduction of SMP30 by lipopolysaccharide (LPS)-treated liver of 13-month-old rat (Jung et al., 2004). Since the hallmark of inflammatory process, in general, increased production of RS, it is rational to associated elevated oxidative stress with neuroinflammatory process (Floyd and Hensley, 2002; Emerit et al., 2004). Moreover, sustained accumulation of various oxidants causes chronic inflammation, which is characterized by the infiltration of leukocytes (Halliwell and Guttweridge, 1999). Therefore, in the present study, we attempted to define the role of SMP30 utilizing the knock-out model in relation to the oxidative status.

2. Materials and methods

2.1. Animal maintenance and tissue preparation

SMP30 deficient mice were previously prepared by the gene targeting (Ishigami et al., 2002). We used 12-months-old male mice in this study. Mice were maintained at 20–23 °C on a 12 h light/12 h dark cycles in controlled environment and fed ad libitum using the procedures approved by The Animal Care and Use Committee of Tokyo Metropolitan Institute of Gerontology.

Cortical tissues were prepared in ice-cold homogenization solution (50 mM potassium phosphate buffer containing 1 mM EDTA, 1 mM para-aminobenzamidine, 1 μM pepstatin, pH 7.2) and disrupted for 20 s with an ultrasonic device. The samples were centrifuged at 12,000 rpm at 4 °C for 30 min. The supernatant was regarded as a whole fraction, and the protein concentration was determined by the method of bicinchoninic acid (BCA) solution.

2.2. Reagents

2′,7′-Dichlorofluorescin diacetate (DCFDA) was obtained from Molecular Probes, Inc. (Eugene, OR, USA). Western blot detection reagent was obtained from Amersham (Amersham, Bucks, UK). Polyvinylidene difluoride (PVDF) membranes were obtained from Millipore Corporation (Bedford, MA, USA). All antibodies and other chemical reagents were purchased from Sigma (St. Louis, MO, USA).

2.3. Assessment of oxidative stress

RS generation was measured as previously described, utilizing a fluorescence probe (Thomas et al., 1992). Briefly, 25 μM DCFDA was added to homogenates for 250 μl of final volume. Changes in fluorescence intensity were measured at 10, 20, 30 and 40 min on a Fluorescence Plate Reader (TECAN, Austria), with excitation and emission wavelengths set at 485 and 530 nm, respectively. The changes of fluorescence intensity were normalized by time (min) and protein concentration.

2.4. Enzyme assays

2.4.1. SOD activity assay

SOD activity was measured using the modified xanthine-oxidase-cytochrome *c* method as described by MaCord and Fridovich (1969). The final concentrations of mixture in e-tube were 50 mM potassium phosphate (pH 7.8), 10 mM xanthine, 0.1% deoxycholate, 50 μM potassium cyanide, 0.1 mM ferricytochrome-*c*, and 0.5 U xanthine oxidase. After well vortexed, the mixture was incubated in heat block at 22 °C for 2 min. Once heated, the reaction was initiated by addition of homogenates (0.03–0.05 mg) into the mixture. The decrease in absorbance at 550 nm was measured for 3 min.

2.4.2. Catalase activity assay

Catalase activity was assayed according to the method (Beers and Sizer, 1953). The final concentrations in the cuvettes were 50 mM potassium phosphate (pH 7.0), 30 mM H_2O_2 and the samples (0.03–0.05 mg). The decrease in absorbance at 240 nm after the addition of the samples was followed spectrophotometrically.

2.4.3. Glutathione peroxidase (GSH-Px) activity assay

GSH-Px activity was assayed with a coupled enzyme system in which glutathione (GSSG) reduction was coupled to NADPH oxidation by glutathione reductase (Lawrence and Burk, 1976). The assay mixture contained 50 mM potassium phosphate (pH 7.5), 1 mM EDTA, 1 mM NaN_3, 1 mM reduced glutathione (GSH), 0.2 mM NADPH, 1 U glutathione reductase and tissue samples (0.05–0.2 mg). After 5 min preincubation (20–25 °C), the reaction was initiated by the addition of 0.25 mM H_2O_2. The decrease in the absorbance at 340 nm was followed spectrophotometrically.

2.4.4. NADPH oxidase activity assay

NADPH consumption was assayed spectrophotometrically at 340 nm (Zhang et al., 2000). The oxidized nucleotides $NADP^+$ do not show any absorbance at 340 nm (Souza et al., 2002). The reaction observed contained the sample (0.05–0.2 mg), diluted to a final 50 mM potassium phosphate (pH 7.5). NADPH (final 1 mM) was added, just before the measurements were started, and followed for 5 min. The decreased absorbance at 340 nm was measured and applied as NADPH oxidase activity.

2.4.5. MPO activity assay

This assay was designed to measure the production of tetramethylbenzidine (TMB) oxidation by MPO/H_2O_2. Samples were mixed with reacting reagent (15 mM TMB, 100 mM sodium acetate, 60 mM hydrogen peroxide). The reaction was monitored at 650 nm for 30 min on a Genios TECAN Spectrophotometer (Austria). Data were expressed mU/mg, protein. One unit of activity is defined as the amount of enzyme that will utilize 1 μmol of hydrogen peroxide/min. In this assay, one milli unit of MPO will cause absorbance change of 0.0114 min^{-1} at a 650 nm.

2.5. Western blot analysis

Western blotting was carried out with whole fractions of the cortical tissues. The samples were boiled for 5 min with a gel-loading buffer (pH 6.8); 0.125 M Tris–HCl, 4% sodium dodecyl sulfate, 20% glycerol, 10% 2-mercaptoethanol, and 0.2% bromophenol blue in a ratio of 1:1. Total protein equivalents for each sample were separated on an SDS—polyacrylamide mini gel using 10 or 15% acrylamide gels at 100 V and transferred to a PVDF membrane at 70 V for 1 h. The membrane was immediately placed into a blocking solution (5% skim milk) at room temperature for 30 min. The membrane was incubated with a diluted primary antibody; SMP30 (1:5000), dityrosine (IC3; 200 ng/ml) (Kato et al., 1998), dinitrophenyl (DNP; 1:1000), SOD (1:2000), catalase (1:1000), Mac-1 (1:1000) and β-tubulin (1:4000) in TBS-Tween buffer at room temperature for 3 h. The membrane was followed by incubation with secondary antibody; polyclonal anti-goat, rabbit, mouse, or rat antibody (1:40,000) in Tween buffer at room temperature for 1 h. Horseradish-conjugate secondary antibody labeling was detected by enhanced chemiluminesence (ECL) Western blotting reagents and analysis (Amersham Bioscience, NJ) following the manufacturer's instructions. Pre-stained blue protein markers were used for molecular weight determination.

2.6. Pathological analysis

Twelve-months-old male WT and SMP30 KO mice were euthanatized and whole brains were removed. Frozen brains were sectioned coronally at 20 μm on a cryostat and were thaw-mounted onto Superfrost PlusTM slides (Fisher, Chicago, IL). Slides were maintained at −20 °C until they were processed for histology. Coronal frozen sections through hippocampus were prepared and stained with cresyl violet (Nissl) for evaluation of neuronal morphology (Wu et al., 2005).

2.7. Statistical analysis

The statistical significance of the differences between WT and SMP30 KO mice was determined by ANOVA with PLSD. Values of $p < 0.05$ were considered statistically significant. Analyses were performed using Statview software®.

3. Results

3.1. Increased RS levels and NADPH oxidase activities in SMP30 KO mice brain

To evaluate the oxidative stress in SMP30 KO mice, we measured total RS levels in the cortex of WT and SMP30 KO mice using DCFDA method (Thomas et al., 1992). Total RS levels in SMP30 KO brain were significantly increased compared to WT mice (Fig. 1A; $p < 0.001$). NADPH oxidase is well known as a major enzyme to generate superoxide anion (Clark et al., 2004). Therefore, we measured NADPH oxidase activities to determine whether RS source enzyme activity was responsible for the elevated total RS levels in the mice. NADPH oxidase activities were consistently elevated with increased RS levels in SMP30 KO brain (Fig. 1B; $p < 0.05$).

3.2. Antioxidant enzyme status

To assess whether the increased oxidative stress is caused by the dysfunction of oxidative defense system in the SMP30 KO brain, we measured the activities and levels of several antioxidative enzymes, including SOD, catalase, and GSH-Px in cortex. However, no marked differences in activities of SOD, catalase, and GSH-Px were detected between WT and SMP30 KO cortex (Fig. 2A). The protein levels of either SOD or catalase were not significantly different between WT and SMP30 KO brain (Fig. 2B). This result demonstrated that antioxidant enzyme status in brain was not affected by SMP30 depletion.

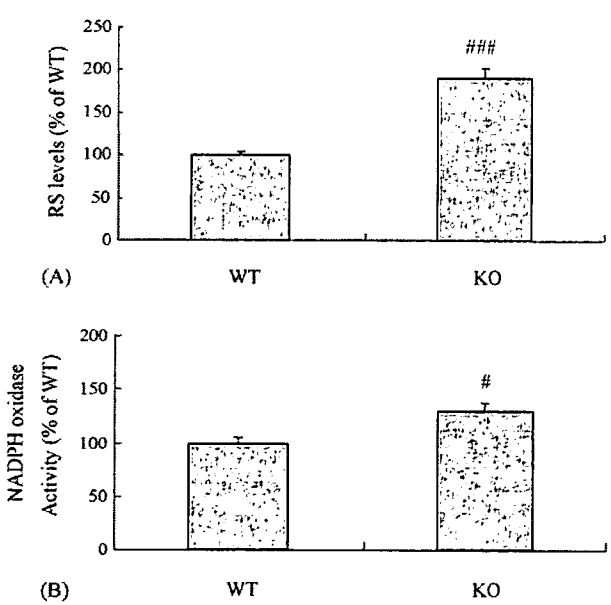

Fig. 1. Levels of reactive species (RS) and activities of NADPH oxidase were increased in SMP30 KO brain. (A) Total RS levels were detected by DCFDA method in cortex of WT and SMP30 KO mice. Levels of RS were significantly increased in SMP30 deficient cortex compared to WT. (B) NADPH oxidase activities were measured by NADPH consumption as substrate at 340 nm spectrophotometer. SMP30 depletion resulted in the elevated activities of NADPH oxidase in the cortex. Each value is the mean ± S.E. of four to five mice in two times experiment with triplicates. As significance, results of one-factor ANOVA: $^{\#}p < 0.05$, $^{\#\#\#}p < 0.001$ vs. WT.

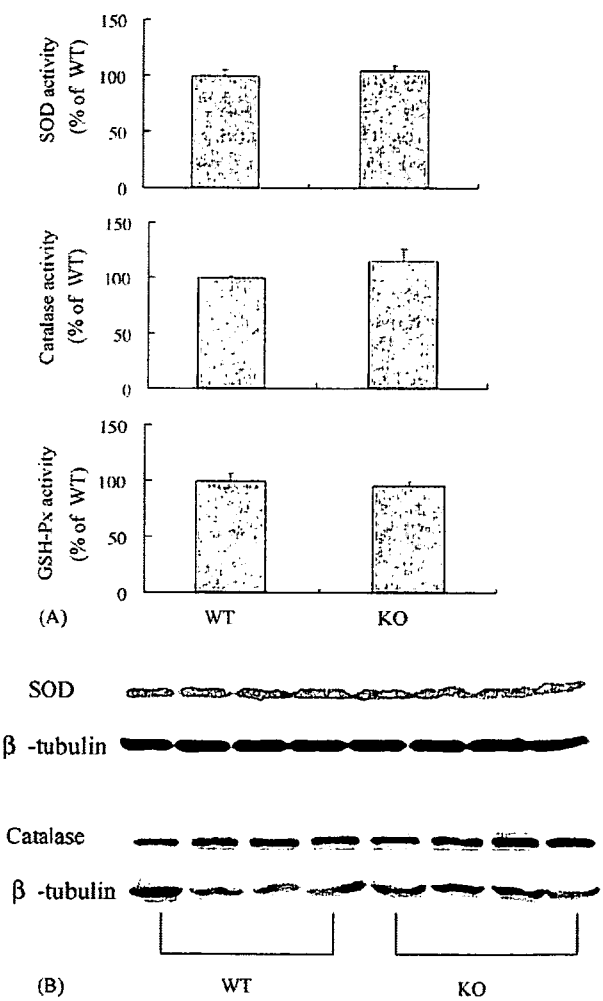

Fig. 2. The antioxidative enzyme status was not altered by SMP30 depletion in the cortex. Activities (A) and protein levels (B) of antioxidant enzymes were examined in the cortical tissues of WT and KO mice. No significant changes were detected in activities of superoxide dismutase (SOD), catalase, and glutathione peroxidase (GSH-Px) between WT and KO mice. (B) Immunoblot analysis showed that protein levels of SOD and catalase were not altered by SMP30 depletion. Levels of β-tubulin used to normalize the levels of protein loaded. Values are expressed as a percentage of WT mice brain and represent means ± S.E. of four mice.

3.3. Enhancement of protein oxidation in SMP30 KO mice brain

We further investigated to evaluate protein oxidation in the cortical tissue from WT and SMP30 KO mice. We examined the dityrosine formation and carbonylation (DNP; dinitrophenyl), because both dityrosine formation (Giulivi et al., 2003) and carbonylation (Liu et al., 2003) was used as markers of protein oxidation. We were able to confirm that SMP30 protein expression was completely depleted in the cortex of SMP30 KO mice (Fig. 3A). Levels of dityrosine and DNP (Fig. 3B; $p < 0.01$ and $p < 0.05$, respectively) were elevated in the cortex of SMP30 KO mice compared to WT mice, indicating that more protein oxidation occurred in SMP30 KO brain. These results suggest that SMP30 deficient brains might be functionally affected by the increased protein oxidation.

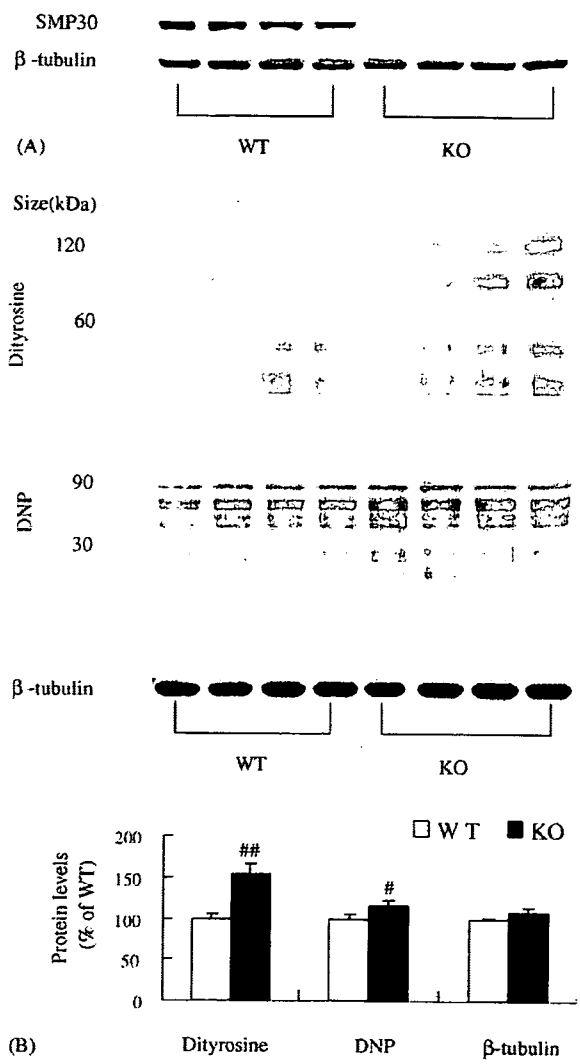

Fig. 3. Protein oxidation was increased in cortex of SMP30 KO mice. (A) Immunoblot analysis showing SMP30 protein levels in WT and KO. (B) Dityrosine formation and carbonylation (DNP) was examined in the mice brain. The cortical homogenates were subjected to immunoblot analysis using anti-dityrosine and anti-DNP. Whole proteins were screened and around size between 60 and 120 kDa of tyrosylated proteins and between 60 and 90 kDa of carbonylated proteins were markedly elevated in SMP30 KO brain compared to WT. Levels of β-tubulin used as protein loading control. Values are expressed protein levels as a percentage of WT mice brain and represent means ± S.E. of four mice. As significance, results of one-factor ANOVA: $^{\#}p < 0.05$, $^{\#\#}p < 0.01$ vs. WT.

3.4. Activated leukocytes in SMP30 KO mice brain

It seems clear that SMP30 KO mice show elevated RS and protein oxidation in the brain, without alteration of antioxidant enzyme status. Since it has been reported that chronic inflammation can be also caused by RS, we hypothesized that activated immune cells were infiltrated into the SMP30 KO brain, which cause unusual release of oxidants. To valid this hypothesis, myeloperoxidase (MPO) activity, a reliable marker for leukocyte recruitment and activation (Morken et al., 2002; Squadrito et al., 2000), was measured in the cortex WT and SMP30 KO mice. The markedly increased MPO activities in SMP30 KO mice indicated the infiltration of activated leukocytes (Fig. 4A). To further confirm our assumption, the level of Mac-1 was determined in the brain homogenates, because Mac-1 is regarded as the key mediator responsible for the migration of neutrophil (Clark et al., 1996). The levels of Mac-1 in SMP30 KO brain were as high as 1.5-fold ($p < 0.01$) of that in WT (Fig. 4B). These results clearly demonstrated the accumulation of leukocytes in the brain tissues taken from SMP30 KO mice, which may be responsible for the elevated RS levels.

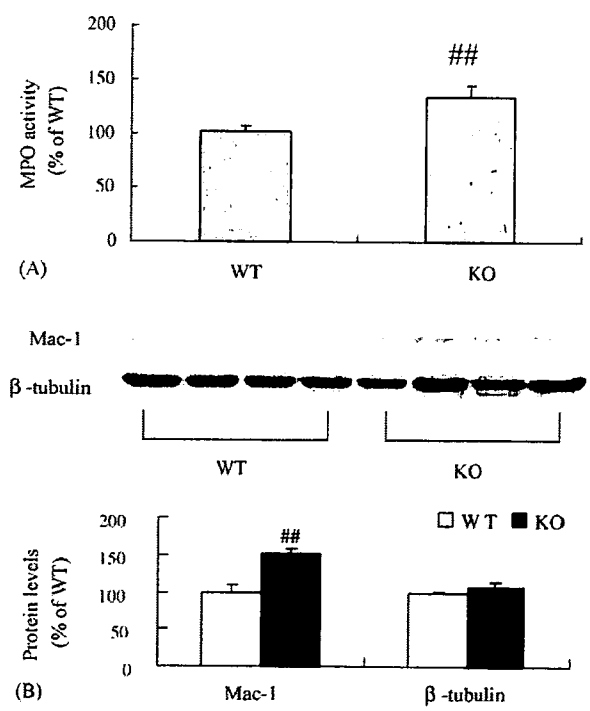

Fig. 4. Infiltration and activation of leukocyte was increased in SMP30 KO brain. (A) MPO activities were measured as an infiltrated leukocyte marker by specific assay in the mice. MPO activities significantly increased in SMP30 KO brain. Values are the mean ± S.E. of four mice. As significance, results of one-factor ANOVA: $^{\#\#}p < 0.01$ vs. WT. (B) The protein levels of Mac-1 were quantified arbitrarily as an activated leukocyte marker by densitometry. Values are expressed protein levels as a percentage of WT mice. As significance, results of one-factor ANOVA: $^{\#\#}p < 0.01$ vs. WT.

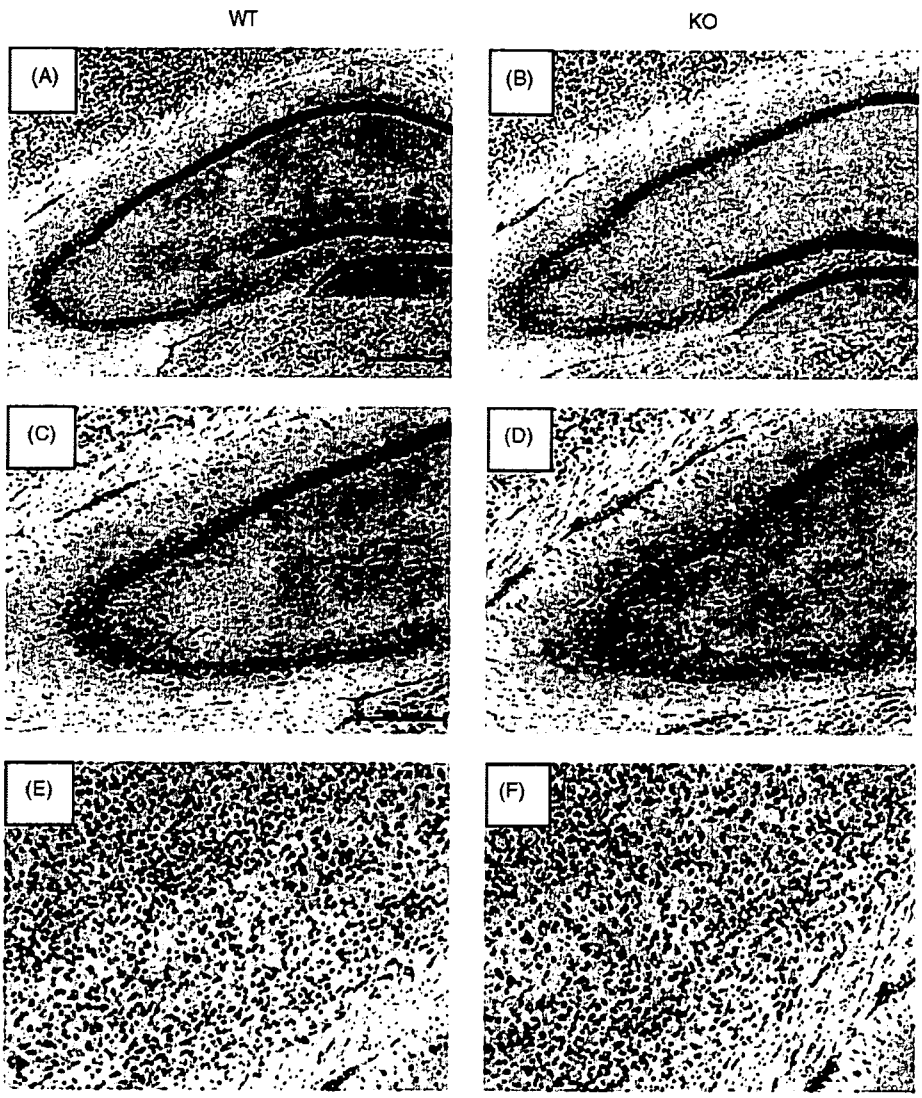

Fig. 5. SMP30 KO mice did not show any neuronal pathology in the brain compared to WT mice. Coronal brain sections of hippocampus were stained with cresyl violet (Nissl) to evaluate neuronal loss and damage. There were no neuronal losses or damages in both WT mice (A, C, E) and SMP30 KO mice (B, D, F). Nissl images of CA1 and CA3 region (C, D) and the cortex (E, F). Scale bar: 100 μm (A, B), 50 μm (C–F).

3.5. Histopathology of SMP30 KO mice brain

We examined the sectioned brain tissues of SMP30 KO mice for the possible pathological changes that might cause the increased oxidative stress and leukocyte infiltration. Nissl stained slides were evaluated for any neuronal damages. The results found that there were no neuronal loss or damage in coronal brain sections of both WT (Fig. 5A, C and E) and SMP30 KO mice (Fig. 5B, D and F). Base on these data, we concluded that increased oxidative status and neutrophil activation in SMP30 KO brains we observed were not likely due to the secondary effects of the pathological changes of the brain.

4. Discussion

Most studies on SMP30 have been focused on the kidney and liver, because expression levels of SMP30 are particularly high in those organs. However, studies on the SMP30's tissue or organ specificity with relatively low levels have not been well studied. The brain is one of those organs with low levels of SMP30, but do express SMP30. The brain is known to be susceptible to damaging effects of oxidative stress due to their high oxygen consumption and relatively low antioxidant capacity (Anderson, 2004). The current study is the first report on the characterization of brain SMP30 utilizing SMP30 KO mice in relation with oxidative status.

We assessed the oxidative status of SMP30 KO brain by measuring several key markers for oxidative stress. Included are: total RS levels for biochemical marker, NADPH oxidase for an enzymatic marker, and MPO activities (as a physiological marker), and found that all are significantly increased in the brain of SMP30 KO mice. Consistent with the oxidatively stressed SMP30 KO brain, there is the increased leukocyte activity as shown in Fig. 4. These observations are consistent

with our preliminary studies with liver and kidney in SMP30 KO mice (data not shown). However, our oxidatively stressed brain was not accompanied with any compensatory changes in activities or protein levels of anti-oxidative defense enzymes in SMP30 KO brain. These results indicate that SMP30 has suppressive action against oxidative stress in the brain without modulating antioxidant enzyme status. This finding raises the possibility of the organ specificity of SMP30 in response to oxidative stress in which case, the SMP30 KO brain seems to have an impaired capacity to induce, i.e. synthesize those scavenging enzymes in response to oxidative stress.

Elevated RS in SMP30 KO brain was verified by detecting protein oxidation; dityrosine and DNP in the mice brain. It is likely that the lack of SMP30 with increased oxidative stress is responsible for the elevated protein oxidation. It was recently reported that protein oxidation by increased oxidative stress has been identified in several neurodegenerative disorders and aging processes. For example, the occurrence of dityrosine in proteins has a wide range of implication in atherosclerosis, inflammation, neurodegenerative disease, and aging (Leeuwenburgh et al., 1999; Hensley et al., 1998). Likewise, toxic carbonyl species have been associated with the pathophysiology of Alzheimer's disease (AD) (Liu et al., 2003). Thus, our findings on the increased dityrosine and carbonylation levels in the brain of SMP30 KO mice highlight a putative important role in the brain as a potent anti-oxidative function.

Other data revealed from the current study support our contention about SMP30's role in the brain. We found that protein levels of Mac-1 as marker of activated leukocyte were increased in SMP30 KO mice. Adhesion and migration of leukocytes is regulated by specific receptor–ligand interactions between intracellular adhesion molecule-1 (ICAM-1) on endothelial cells and a group of Mac-1 glycoproteins on leukocytes (Chao et al., 2000). To probe the infiltration of migrated leukocyte, we measured MPO activity in the mice, because identification of MPO can be used as neutrophil infiltration. We also found that MPO activities are consistent with increased levels of Mac-1 protein in SMP30 KO mice brain. These results indicate that the increased MPO activities are further confirming the status of oxidative stress in SMP30 KO mice brain.

One could suspects that the infiltration of neutrophil and increased oxidative stress were associated with the pathological processes in these KO mouse brain. However, our gross microscopic analysis of the brain shown in Fig. 5 revealed no discernable differences in sizes and shapes of hippocampus and cortex in SMP30 KO mice compared to wild type mice. In addition, histopathological analysis with Nissl staining indicates that there were no neuronal losses or damages in SMP30 KO mice compared to WT mice. Therefore, it is not likely that increased oxidative stress and leukocyte infiltration in SMP30 KO brains we observed in these KO mice are from the secondary effects of brain lesion. However, it is still probably true that SMP30 KO mice are more susceptible to pathological insults and vulnerable to various stresses due to the weakened anti-oxidative defenses.

Putting together, our findings suggest that SMP30 plays an important neuroprotective role in suppressing oxidative stress by modulating activation and infiltration of leukocytes, but without compensatory increases in endogenous oxidative defense enzymes.

Acknowledgements

The authors gratefully thank Dr. Yoji Kato (School of Human Science and Environment, University of Hyogo, Himeji, Hyogo, Japan) for kind providing the anti-dityrosine antibody.

We are grateful to the 'Aging Tissue Bank' for distributing the SMP30 KO mice brain.

References

Anderson, J.K., 2004. Oxidative stress in neurodegeneration: cause or consequence? Nature 10, S18–S25.

Beers Jr., R.F., Sizer, I.W., 1953. Catalase assay with special reference to manometric methods. Science 117, 710–712.

Clark, R.S., Carlos, T.M., Schiding, J.K., 1996. Antibodies against Mac-1 attenuate neutrophil accumulation after traumatic brain injury in rats. J. Neurotrauma. 13, 333–341.

Clark, R.A., Epperson, T.K., Valente, A., 2004. Mechanisms of activation of NADPH oxidases. Jpn. J. Infect. Dis. 57, S22–S23.

Chao, G., Hoff, J.T., Keep, R., 2000. Acute inflammatory reaction following experimental intracerebral hemorrhage in rat. Brain Res. 871, 57–65.

Emerit, J., Edeas, M., Bricare, F., 2004. Neurodegenerative diseases and oxidative stress. Biomed. Pharmacother. 58, 39–46.

Feng, D., Kondo, Y., Ishigami, A., 2004. Senescence marker protein 30 as a novel antiaging molecule. Ann. N.Y. Acad. Sci. 1019, 360–364.

Fujita, T., Uchida, K., Maruyama, N., 1992. Purification of senescence marker protein-30 (SMP30) and its independent decrease with age in the rat liver. Biochim. Biophys. Acta 1116, 122–128.

Fujita, T., Shirasawa, T., Maruyama, N., 1999. Expression and structure of senescence marker protein-30(SMP30) and its biological significance. Mech. Age. Dev. 107, 271–280.

Fukaya, Y., Yamaguchi, M., 2004. Regucalcin increases superoxide dismutase activity in rat liver cytosol. Biol. Pharm. Bull. 27, 1444–1446.

Floyd, R.A., Hensley, K., 2002. Oxidative stress in brain aging implications for therapeutics of neurodegenerative disease. Neurobiol. Age. 23, 795–807.

Giulivi, C., Traaseth, N.J., Davies, K.J.A., 2003. Tyrosine oxidation products: analysis and biological relevance. Amino Acids 25, 227–232.

Halliwell, B., Guttweridge, J., 1999. Free Radical in Biology and Medicine, third ed. Oxford Press, Oxford, UK.

Hensley, K., Maidt, M.L., Yu, Z.Q., 1998. Electrochemical analysis of protein nitro-tyrosine and dityrosine in the Alzheimer brain indicates region-specific accumulation. J. Neurosci. 18, 8126–8132.

Izumi, T., Tsurusaki, Y., Yamaguchi, M., 2003. Suppressive effect of endogenous regucalcin on nitric oxide synthase activity in cloned rat hepatoma H4-II-E cells overexpressing regucalcin. J. Cell. Biochem. 89, 800–807.

Izumi, T., Yamaguchi, M., 2004. Overexpression of regucalcin suppresses cell death in cloned rat hepatoma H4-II-E cells induced by tumor necrosis factor-alpha or thapsigargin. J. Cell. Biochem. 92, 296–306.

Ishigami, A., Fujita, T., Simbula, G., et al., 2001. Regulatory effects of senescence marker protein 30 on the proliferation of hepatocytes. Pathol. Int. 51, 491–497.

Ishigami, A., Fujita, T., Handa, S., et al., 2002. Senescence marker protein-30 knockout mouse licer is highly susceptible to TNF-α- and Fas-mediated apoptosis. Am. J. Pathol. 161, 1273–1281.

Ishigami, A., Kondo, Y., Nanba, R., et al., 2004. SMP30 deficiency in mice causes an accumulation of neutral lipids and phospholipids in the liver and shortens the life span. Biochem. Biophys. Res. Commun. 315, 575–580.

Ichikawa, E., Yamaguchi, M., 2004. Regucalcin increase superoxide dismutase activity in the heart cytosol of normal and regucalcin transgenic rats. Int. J. Mol. Med. 14, 691–695.

Jung, K.J., Ishigami, A., Maruyama, N., et al., 2004. Modulation of gene expression of SMP30 by LPS and calorie restriction during aging process. Exp. Gerontol. 39, 1169–1177.

Kato, Y., Maruyama, W., Naoi, M., 1998. Immunohistochemical detection of dityrosine in lipofusin pigments in the aged human brain. FEBS Lett. 439, 231–234.

Liu, Q., Raina, A.K., Smith, M.A., 2003. Hydroxynonenal, toxic carbonyls, and Alzheimer disease. Mol. Aspects Med. 24, 305–313.

Leeuwenburgh, C., Hansen, P.A., Holoszy, J.O., 1999. Oxidized amino acids in the urine of aging rats. Am. J. Physiol. 45, R128–R135.

Lawrence, R.A., Burk, R.F., 1976. Glutathione peroxidase activity in selenium deficient rat liver. Biochem. Biophys. Res. Commun. 71, 952–958.

MaCord, J.M., Fridovich, I., 1969. The utility of superoxide dismutase in studying free radical reactions. I. Radicals generated by the interaction of sulfite, dimethyl sulfoxide, and oxygen. J. Biol. Chem. 244, 6056–6063.

Morken, J.J., Warren, K.U., Xie, Y., 2002. Epinephrine as a mediator of pulmonary neutrophil sequestration. Shock 18, 46–50.

Maruyama, N., Ishigami, A., Kuramoto, M., et al., 2004. Senescence marker protein-30 knockout mouse as an aging model. Ann. N.Y. Acad. Sci. 1019, 383–387.

Matsuyama, S., Kitamura, T., Enomoto, N., et al., 2004. Senescence marker protein-30 regulates Akt activity and contributes to cell survival in Hep G2 cells. Biochem. Biophys. Res. Commun. 321, 386–390.

Thomas, P., Herbert, D.G., James, P.K., 1992. Production of reactive oxygen by mitochondrial from normoxic and hypoxic rat heart tissue. Free Radic. Biol. Med. 13, 289–297.

Souza, H.P., Liu, X., Zweier, J.L., 2002. Quantitation of superoxide generation and substrate utilization by vascular NAD(P)H oxidase. Am. J. Physio. Heart Circ. Physiol. 282, H466–H474.

Squadrito, F., Alrtavilla, D., Squadrito, G., 2000. Tacrolimus limits polymorphonuclear leukocyte accumulation and protects against myocardial ischemia-reperfusion injury. J. Mol. Cell Cardiol. 32, 429–440.

Wu, G., Lu, Z., Wang, J., 2005. Enhanced susceptibility to kainate induced seizures, neuronal apoptosis and death in mice lacking gangliotetraose ganglioside: protection with LIGA 20 a membrane permeant analog of GM1. J. Neurosci. 25, 11014–11022.

Zhang, Z., Yu, J., Stanton, R., 2000. A method for determination of pyridine nucleotide using a single extract. Anal. Biochem. 285, 163–167.

Senescence Marker Protein-30 Protects Mice Lungs from Oxidative Stress, Aging, and Smoking

Tadashi Sato, Kuniaki Seyama, Yasunori Sato, Hiroaki Mori, Sanae Souma, Taeko Akiyoshi, Yuzo Kodama, Takanori Mori, Sataro Goto, Kazuhisa Takahashi, Yoshinosuke Fukuchi, Naoki Maruyama, and Akihito Ishigami

Department of Respiratory Medicine, Juntendo University, School of Medicine; Department of Molecular Pathology, Tokyo Metropolitan Institute of Gerontology, Tokyo; and Department of Biochemistry, Faculty of Pharmaceutical Sciences, Toho University, Chiba, Japan

Rationale: **Senescence marker protein-30 (SMP30) is a multifunctional protein providing protection to cellular functions from age-associated deterioration. We previously reported that SMP30 knockout (SMP30Y/−) mice are capable of being novel models for senile lung with age-related airspace enlargement and enhanced susceptibility to harmful stimuli.**

Objectives: **Aging and smoking are considered as major contributing factors for the development of pulmonary emphysema. We evaluated whether SMP30Y/− mice are susceptible to oxidative stress associated with aging and smoking.**

Methods: **Age-related changes of protein carbonyls in lung tissues from the wild-type (SMP30Y/+) and SMP30Y/− mice were evaluated. Both strains were exposed to cigarette smoke for 8 wk. Histopathologic and morphologic evaluations of the lungs, protein carbonyls and malondialdehyde in the lung tissues, total glutathione content in the bronchoalveolar lavage fluid, and degree of apoptosis of lung cells were determined.**

Measurements and Main Results: **In the lungs of SMP30Y/− mice, protein carbonyls tended to increase with aging and were significantly higher than the age-matched SMP30Y/+ mice. Cigarette smoke exposure generated marked airspace enlargement (23.3% increase of the mean linear intercepts) with significant parenchymal destruction in the SMP30Y/− mice but not in the SMP30Y/+ mice (5.4%). The protein carbonyls, malondialdehyde, total glutathione, and apoptosis of lung cells were significantly increased after 8-wk exposure to cigarette smoke in the SMP30Y/− mice.**

Conclusions: **Our results suggest that SMP30 protects mice lungs from oxidative stress associated with aging and smoking. The SMP30Y/− mice could be useful animal models for investigating age-related lung diseases, including cigarette smoke–induced pulmonary emphysema.**

Keywords: aging; oxidative stress; pulmonary emphysema; senescence marker protein-30; smoking

Senescence marker protein-30 (SMP30), a 34-kD protein originally identified from the rat liver, is a novel molecule that decreases with age in an androgen-independent manner, suggesting its possible role in age-related physiologic and pathologic conditions (1–3). We demonstrated that SMP30 is widely expressed in vertebrates and that the amino acid alignment is highly conserved (2, 4). In mice, SMP30 transcripts are detected in various organs, including the liver, kidney, cerebrum, testis, and lung (5). In humans, the SMP30 gene is located in the p11.3–q11.2 segment of the X chromosome (6). To clarify the physiologic role of SMP30 in age-associated organ disorders, the SMP30 knockout (SMP30Y/−) mouse was developed with gene targeting from C57BL6 mice (7). We revealed that SMP30Y/− mice are viable and fertile but have reduced weight gain and shorter life span than the wild-type (SMP30Y/+) mice (8). Hepatocytes isolated from SMP30Y/− mice were shown to be highly susceptible to tumor necrosis factor-α and Fas-mediated apoptosis (7). Furthermore, exogenously induced SMP30 was shown to increase Ca^{2+} efflux by activating the calmodulin-dependent Ca^{2+} pump in HepG2 cells and thus to confer resistance to cell death caused by an increase in intracellular Ca^{2+} concentration (9). These findings suggest that SMP30 protects cells and organs from various injuries during the course of life.

There are many studies concerned with the relationship between aging and oxidative stress. Moderate oxidative stress may gradually develop with age because plasma levels of lipoperoxidation products and antioxidant enzyme activities in red blood cells increase with aging, whereas plasma levels of nutritional antioxidants decrease (10). The lungs are persistently exposed to oxidants generated endogenously from phagocytes and other cell types or exogenously from air pollutants or cigarette smoke (11). Pulmonary emphysema is an age-related lung disease that occurs after a prolonged period of cigarette smoking. Because cigarette smoke contains around 10^{17} oxidant molecules per puff and generates oxidant/antioxidant imbalance in the lungs, oxidative stress is postulated to play an important role in the pathogenesis of emphysema (11). In patients with chronic obstructive pulmonary disease, biomarkers of oxidative stress, such as protein carbonyls and lipid peroxidation products, are reported to be elevated in the lungs (12) and respiratory muscles (13).

We previously reported that SMP30Y/− mice develop peripheral airspace enlargement without alveolar destruction and may thus be a novel model for senile lung (5). We hypothesized that SMP30Y/− mice may be susceptible to oxidative stress with aging. Furthermore, SMP30Y/− mice may be vulnerable to cigarette smoke exposure and generate pulmonary emphysema. In this study, we investigated the age-related changes of protein carbonyls in the lungs of SMP30Y/− and SMP30Y/+ mice and pathologically evaluated the effect of cigarette smoke exposure to the lungs and biomarkers of oxidative stress.

METHODS

Animals

We used SMP30Y/− and SMP30Y/+ mice to investigate the age-related changes of mice lungs with 1-, 3-, 6-, and 12-mo-old mice (n = 5 for each group). We used 3-mo-old mice (n = 6 for each group) for the smoking experiment. Animal experimentation was approved by the

(Received in original form November 28, 2005; accepted in final form May 24, 2006)

Supported by Grant-in-Aid for Scientific Research No. 13470130 (Y.F.) and No. 15390259 (Y.F.); by the High Technology Research, Center Grant from the Ministry of Education, Culture, Sports, Science, and Technology, Smoking Science Foundation No. FP00404086 (N.M.); by a grant to the Respiratory Failure Research Group from the Ministry of Health, Labor and Welfare, Japan (K.S.); and by the Institute for Environmental and Gender-Specific Medicine, Juntendo University, Graduate School of Medicine (K.S.).

Correspondence and requests for reprints should be addressed to Tadashi Sato, M.D., Department of Respiratory Medicine, Juntendo University, School of Medicine, 2-1-1 Hongo, Bunkyo-Ku, Tokyo 113-8421, Japan. E-mail: satotada@med.juntendo.ac.jp

This article has an online supplement, which is accessible from this issue's table of contents at www.atsjournals.org

Am J Respir Crit Care Med Vol 174. pp 530–537, 2006
Originally Published in Press as DOI: 10.1164/rccm.200511-1816OC on May 25, 2006
Internet address: www.atsjournals.org

Animal Care and Use Committee of Tokyo Metropolitan Institute of Gerontology and by Juntendo University, School of Medicine.

Preparation and Morphologic Evaluation of the Lungs

Mice were killed, and the lungs were processed as described previously (14). The lungs were lavaged with 0.5 ml of phosphate-buffered saline through an intratracheal cannula four times. The bronchoalveolar lavage fluid (BALF) was pooled, and total cell counts and cell populations in each BALF specimen were determined. The BALF was centrifuged, and the supernatant was collected for biochemical analysis.

Airspace size was assessed by determining the mean linear intercepts (MLI) according to the method previously described (15). The destructive index (DI) was determined to evaluate the severity of alveolar wall destruction (16). A DI value greater than 10% was considered to have significant destruction of the lung parenchyma (17).

Determination of Protein Carbonyls in the Lungs

The measurement of protein carbonyls in the supernatant of lung homogenates was conducted with a spectrophotometer as described previously (18–20). To confirm the specificity of the reaction of the proteins with 2,4-dinitrophenylhydrazine (DNPH), the lung extracts of SMP30Y/− mice were pretreated with sodium borohydride to reduce the carbonyls in the experiment as described previously (20). The absorbance of the spectrophotometric measurement of carbonyls was reduced to 16% with treatment, confirming the validity of the method.

Immunohistochemical Staining for Protein Carbonyls in the Lungs

Protein carbonyls were identified immunohistochemically with paraffin-embedded lung sections using specific antiserum against DNPH prepared with rabbits as described previously (20). The sections were incubated with DNPH solution for 30 min and then with anti-DNPH antibody for 1 h at room temperature. The sections were incubated with biotinylated anti-rabbit IgG antibody (Vector, Burlingame, CA). Antibody binding was detected using the Elite ABC Kit (Vector) and 3,3-diaminobenzidine tetrahydrochloride as the chromogen according to the manufacturer's instructions. As a negative control, the sections were incubated in 2% HCl without DNPH for 30 min before incubation with the primary antibody or in a solution containing 2% bovine serum albumin and 2% normal goat serum instead of the polyclonal anti-DNPH antibody. All the sections were counterstained with hematoxylin.

Chronic Exposure to Cigarette Smoke

Mice were exposed to cigarette smoke for 8 wk using the commercially marketed Peace nonfilter cigarettes (29 mg of tar and 2.5 mg of nicotine per cigarette; Japan Tobacco, Inc., Tokyo, Japan) and the Tobacco Smoke Inhalation Experiment System for small animals (Model SIS-CS; Shibata Scientific Technology, Tokyo, Japan) as described previously (14). We used 2.5% cigarette smoke diluted with compressed air (mass concentration of total particulate matter, 40.6 mg/m^3). Three-month-old mice were exposed to diluted cigarette smoke (study group) or fresh air (control group) for 30 min/d, 5 d/wk, and for 8 wk.

Determination of Malondialdehyde in the Lungs

The measurement of malondialdehyde (MDA) in the supernatant of lung homogenates was performed using the Lipid Peroxidation Assay Kit (Calbiochem, San Diego, CA) according to the manufacturer's instructions.

Determination of Glutathione in the BALF

Total glutathione and oxidized glutathione contents in the BALF supernatants were measured using the Total Glutathione Quantification Kit (Dojindo Molecular Technologies, Kumamoto, Japan) according to the manufacturer's instructions.

Evaluation of Apoptosis with Immunohistochemistry for Anti–Single-stranded DNA and Anti–Activated Caspase-3 Antibodies

Apoptosis of lung cells was examined with immunohistochemistry using a rabbit polyclonal antibody against the single-stranded DNA (ssDNA; Dako Cytomation, Carpinteria, CA) and anti–activated caspase-3 (Cell Signaling, Beverly, MA) as described previously (14).

Protein Assays

Total protein concentration was measured using the BCA Protein Assay Kit (Pierce, Rockford, IL) according to the manufacturer's instructions.

Statistical Analysis

The statistical significance of the data was determined using analysis of variance followed by Tukey's multiple comparison test. When applicable, the Mann-Whitney test was used. A p value of less than 0.05 was considered significant.

RESULTS

Age-related Changes in Body Weight, Morphometry of the Lungs, and Protein Carbonyls

Body weights increased with age in the SMP30Y/+ and SMP30Y/− mice, and there were no significant changes between both strains up to 6 mo of age. At 12 mo of age, the body weight of the SMP30Y/− mice were significantly less than that of the SMP30Y/+ mice (Table 1). Compared with the SMP30Y/+ mice, the SMP30Y/− mice had significantly greater MLI from 3 to 12 mo of age. There was a significant increase of MLI with aging in the lungs of the SMP30Y/− mice. On the other hand, the DI scores in both groups at every age were less than 10%, and no significant differences between the groups were recorded (Table 1). There were no inflammatory findings in the alveoli in both groups on histologic examination (data not shown).

We assessed protein oxidation in the lungs of SMP30Y/+ and SMP30Y/− mice by measuring the protein carbonyls, which are known as sensitive biomarkers of oxidative stress (21). In the lungs of SMP30Y/− mice, protein carbonyls were significantly increased in comparison with those of age-matched SMP30Y/+ mice. In addition, protein carbonyls tended to increase with age and significantly increased at 12 mo of age as compared with 1 mo of age (Figure 1). We performed immunohistochemistry with anti-DNPH antibody to detect the localization of protein carbonyls in the lungs and demonstrated that the majority of the protein carbonyls was evenly distributed and diffused in both strains but was apparently stronger in the SMP30Y/− mice (Figure 2).

Effect of Cigarette Smoke Exposure on the Morphometry of the Lungs

The body weights did not change significantly between the SMP30Y/+ and SMP30Y/− mice before and after exposure to

TABLE 1. AGE-RELATED CHANGES OF BODY WEIGHT AND LUNG MORPHOMETRY IN SMP30Y/+ AND SMP30Y/− MICE

	1 mo	3 mo	6 mo	12 mo
BW, g				
SMP30Y/+	22.1 ± 0.6	29.2 ± 0.9	33.3 ± 2.1	41.1 ± 2.3
SMP30Y/−	22.0 ± 0.6	28.0 ± 0.7	32.1 ± 3.2	37.6 ± 1.0*
MLI, μm				
SMP30Y/+	57.4 ± 4.4	57.7 ± 3.3	60.7 ± 1.6	61.5 ± 3.9
SMP30Y/−	58.6 ± 2.9	62.0 ± 1.4*†	67.1 ± 2.3*‡	67.6 ± 3.9*‡
DI, %				
SMP30Y/+	3.8 ± 0.7	4.2 ± 0.5	4.1 ± 1.1	4.5 ± 0.8
SMP30Y/−	4.2 ± 0.8	4.3 ± 0.5	4.5 ± 0.9	4.9 ± 1.0

Definition of abbreviations: BW = body weight; DI = destructive index; MLI = mean linear intercepts.

Data are presented as mean ± SD (n = 5 for each group).

* $p < 0.05$ versus age-matched SMP30Y/+ mice.

† $p < 0.05$ versus SMP30Y/− mice at 1 mo of age.

‡ $p < 0.001$ versus SMP30Y/− mice at 1 mo of age.

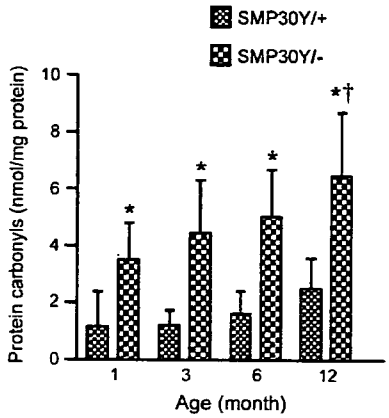

Figure 1. Age-related changes of protein carbonyls in the lungs of SMP30Y/+ and SMP30Y/− mice. In the lungs of the SMP30Y/− mice, protein carbonyls tended to increase with age (†$p < 0.05$, compared with 1 mo of age) and were significantly greater than those of the age-matched SMP30Y/+ mice (*$p < 0.05$). Values are presented as mean ± SD ($n = 5$ for each group).

cigarette smoke for 8 wk. In addition, exposure to cigarette smoke had no influence on body weight gain in both strains as compared with the air-exposed groups (data not shown).

Chronic exposure to cigarette smoke increased total cell counts in the BALF of both groups. No significant differences were observed in cell populations between air- and smoke-exposed mice of both strains. The total protein concentration in the BALF increased significantly in the SMP30Y/− mice after chronic exposure to cigarette smoke but did not increase in the SMP30Y/+ mice. The smoke-exposed SMP30Y/− mice demonstrated significantly higher levels of protein concentration in BALF than the smoke-exposed SMP30Y/+ mice (Table 2).

Chronic exposure to cigarette smoke for 8 wk generated pulmonary emphysema in the SMP30Y/− mice but not in SMP30Y/+ mice. Histologic specimens of the lung tissues of smoke-exposed SMP30Y/− mice revealed marked airspace enlargement (i.e., an increase of MLI) accompanied with disruption of alveolar wall (i.e., an increase of DI; Figures 3 and 4). Morphometric examination of the lung specimen revealed that MLI was significantly greater in the smoke-exposed SMP30Y/− mice than in the air-exposed SMP30Y/− and SMP30Y/+ mice (Figure 4A): MLI increased to 23.3% in the SMP30Y/− mice after exposure to cigarette smoke and 5.4% for the SMP30Y/+ mice. Moreover, DI increased to more than 10%, a cut-off value indicating the occurrence of significant alveolar wall destruction (17), in the lungs from smoke-exposed SMP30Y/− mice, whereas no significant increase was observed in the SMP30Y/+ mice (Figure 4B).

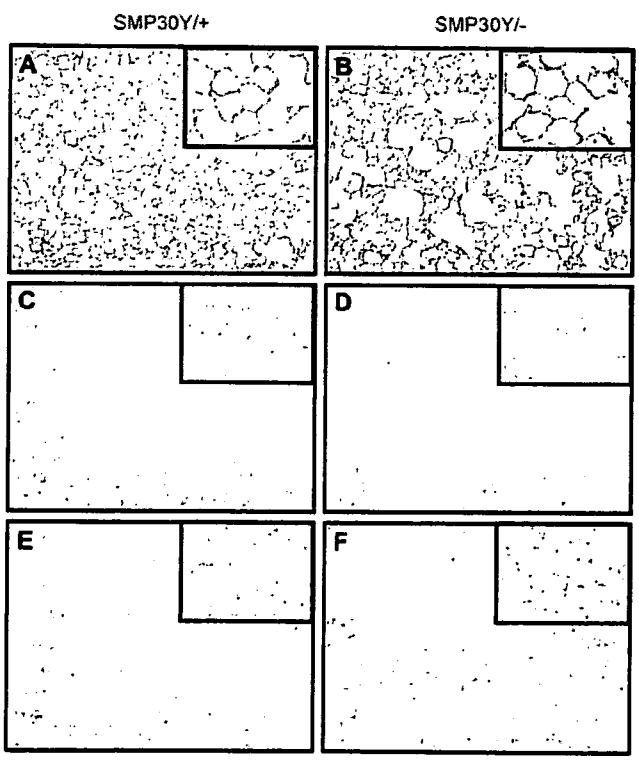

Figure 2. Immunohistochemistry for protein carbonyls in the lungs of SMP30Y/+ (*A*, *C*, and *E*) and SMP30Y/− (*B*, *D*, and *F*) mice (original magnification: ×100). *Insets* are magnified views of the alveolar region (×400). Anti–2,4-dinitrophenylhydrazine (-DNPH) antibody analysis revealed that protein carbonyls were largely evenly and diffusely distributed in the lung tissues of both strains but apparently were stronger in the SMP30Y/− mice (*A* and *B*). As a control for immunostaining of the lung tissues, avoiding the derivatization process (*C* and *D*) and removing primary anti-DNPH antibody (*E* and *F*) resulted in the elimination of positive immunostaining.

Effect of Cigarette Smoke Exposure on Oxidative Stress in the Lungs

To investigate the effect of chronic cigarette smoke exposure on oxidative injury in the lungs, we measured protein carbonyls in the lungs of SMP30Y/+ and SMP30Y/− mice after exposure to air or cigarette smoke (Figure 5). Protein carbonyls tended to increase in the lungs of both strains after cigarette smoke exposure, although no significant statistical difference was noted ($p = 0.08$ and 0.07 between air and smoke exposure in SMP30Y/+ and SMP30Y/− mice, respectively). Protein carbonyls were significantly increased in the lungs of smoke-exposed SMP30Y/− mice than those of the smoke-exposed SMP30Y/+ mice. We also performed immunohistochemistry with anti-DNPH antibody on lung specimens from both strains after chronic exposure to cigarette smoke. Anti-DNPH antibody demonstrated an even and diffuse distribution of protein carbonyls in the lungs of both strains after exposure to cigarette smoke (data not shown), indicating that chronic smoke exposure seems to increase oxidative stress evenly throughout the lungs.

We assessed lipid peroxidation in the lungs by measuring MDA (Figure 6), which is known as one of the end products derived from peroxidation of polyunsaturated fatty acids and related esters (22). Baseline levels of MDA in the lung tissues from both strains (air-exposed) were almost identical. However, MDA significantly increased in the lungs of the SMP30Y/− mice after chronic cigarette smoke exposure, whereas no increase was demonstrated in the lungs of the SMP30Y/+ mice. We did not use the conventional thiobarbituric acid method to measure the MDA because of low specificity of this method. Instead, we used a method that allows us to assay MDA selectively by reacting with N-methyl-2-phenylindole in HCl, eliminating the potential inclusion of 4-hydroxylalkenals and alkanals in the measurement. The reaction produces a chromophore with maximum absorption at 586 nm, whereas the reaction with alkanals forms a product with maximum absorption at 505 nm (23).

We measured the content of total glutathione in BALF (Figure 7) because it is widely recognized as a major antioxidant in the lungs (24, 25). In SMP30Y/− mice, baseline level of total glutathione in BALF tended to be greater than that of the SMP30Y/+ mice, but no statistical significance was detected ($p = 0.06$).Chronic cigarette smoke exposure markedly upregulated the amount of total glutathione in BALF from the SMP30Y/− mice ($p < 0.05$), whereas no effect of smoke exposure on the glutathione level was revealed in the SMP30Y/+ mice

TABLE 2. EFFECT OF CHRONIC CIGARETTE SMOKE EXPOSURE ON BRONCHOALVEOLAR LAVAGE FLUID ANALYSES IN SMP30Y/+ AND SMP30Y/− MICE

	SMP30Y/+		SMP30Y/−	
	Air Exposure	Smoke Exposure	Air Exposure	Smoke Exposure
Total cell count ($\times 10^5$)	0.5 ± 0.2	1.5 ± 0.3*	0.9 ± 0.5	1.9 ± 0.7†‡
Cell differentiation				
Macrophages, %	90.3 ± 7.3	88.8 ± 4.0	87.0 ± 10.2	84.0 ± 9.7
Neutrophils, %	1.0 ± 1.1	1.0 ± 1.1	0.7 ± 1.0	1.2 ± 1.3
Lymphocytes, %	8.5 ± 6.4	9.7 ± 3.7	12.0 ± 9.2	14.2 ± 8.4
Total protein, μg/ml	128.4 ± 106.8	93.0 ± 37.2	145.0 ± 84.3	282.9 ± 63.1‡§¶

Data are presented as mean ± SD (n = 6 for each group).
* $p < 0.001$ versus SMP30Y/+ mice exposed to air.
† $p < 0.01$ versus SMP30Y/+ mice exposed to air.
‡ $p < 0.05$ versus SMP30Y/− mice exposed to air.
§ $p < 0.05$ versus SMP30Y/+ mice exposed to air.
¶ $p < 0.001$ versus SMP30Y/+ mice exposed to cigarette smoke.

($p = 0.79$). We were able to detect oxidized glutathione in BALF from the cigarette smoke–exposed SMP30Y/− mice group but not from the other groups (i.e., less than the detection limit). The amount of oxidized glutathione detected in smoke-exposed SMP30Y/− mice was 7.91 nmol/mg protein (7.95% of total glutathione content).

Effect of Cigarette Smoke Exposure on Apoptosis of Lung Cells

Apoptosis of lung cells was analyzed to investigate the mechanisms of cigarette smoke-induced emphysema in the SMP30Y/− mice. Immunohistochemical examination using anti–single-stranded DNA antibody revealed that apoptosis was widely detected in bronchial and bronchiolar epithelial cells and alveolar septal cells and was significantly increased in all areas of the lungs of the cigarette smoke–exposed SMP30Y/− mice compared with the other groups (Figures 8A and 8B). On the other hand, there was no significant difference in the ratio of apoptotic nuclei detected between the air- and smoke-exposed SMP30Y/+ mice ($p = 0.09$) and between the air-exposed SMP30Y/+ and SMP30Y/− mice ($p = 0.07$). Chronic cigarette smoke–induced increase in apoptosis was further confirmed with immunohistochemical analysis of caspase-3: Activated caspase-3 was detected in the lungs of cigarette smoke–exposed SMP30Y/− mice (Figure 8C) but not in the other groups (data not shown).

DISCUSSION

We have demonstrated that the oxidative stress in the lungs is greater in the SMP30Y/− mice than the SMP30Y/+ mice and tends to gradually increase in the SMP30Y/− mice as determined from measuring the protein carbonyls, one of the biomarkers for oxidative stress (26, 27), in the lungs. We did not measure the age-related changes of lipid peroxidation as another biomarker for oxidative stress and glutathione as a major antioxidant in BALF. At 5 mo of age, however, there was no significant statistical difference between SMP30Y/+ and SMP30Y/− mice in lipid peroxidation of the lungs (Figure 6; $p = 0.76$) and glutathione in BALF (Figure 7; $p = 0.06$). In contrast, chronic cigarette smoke exposure for 8 wk resulted in a marked increase of lipid peroxidation and up-regulation of glutathione, with the tendency of a greater increase of protein carbonyls in the SMP30Y/− mice, but it did not generate significant influence on these biomarkers of oxidative stress in the SMP30Y/+ mice.

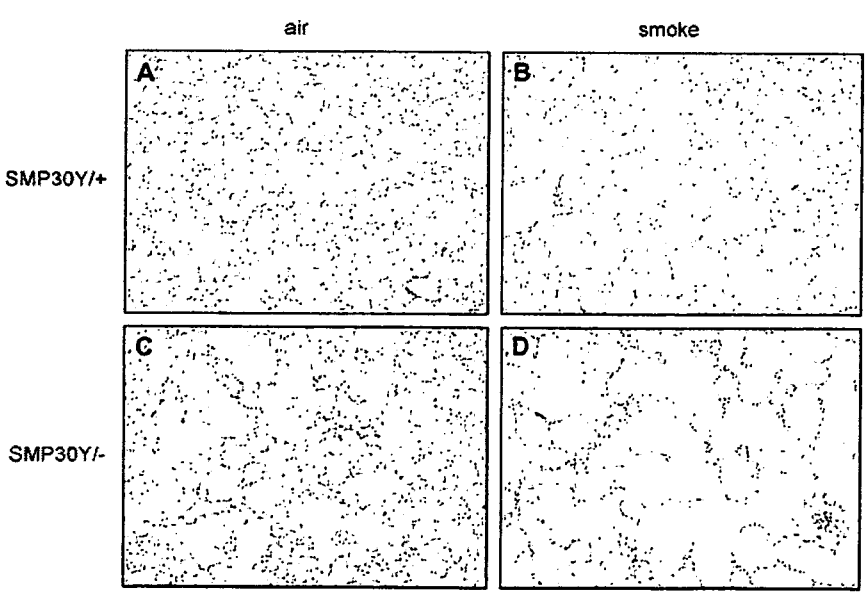

Figure 3. Histologic findings of the lungs of SMP30Y/+ and SMP30Y/− mice after chronic cigarette smoke exposure (hematoxylin–eosin staining; original magnification, ×50). (*A* and *B*) SMP30Y/+ mice exposed to air and cigarette smoke, respectively. (*C* and *D*) SMP30Y/− mice, exposed to air and cigarette smoke, respectively. The lungs of the SMP30Y/− mice exposed to cigarette smoke revealed marked airspace enlargement and alveolar wall destruction (*D*).

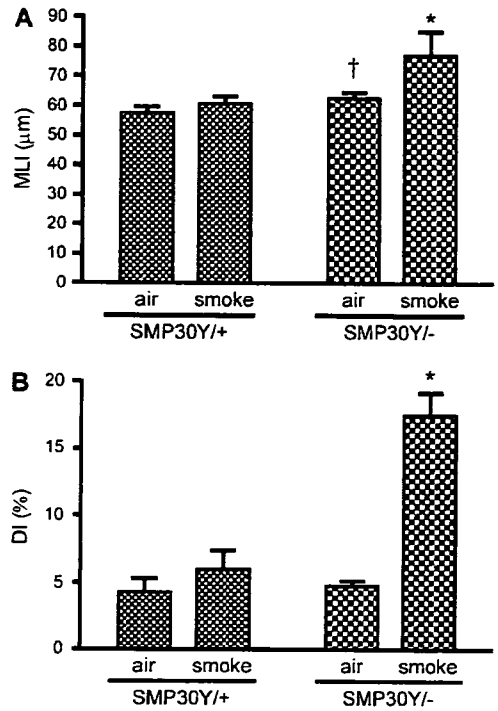

Figure 4. Morphometric findings of the lungs of SMP30Y/+ and SMP30Y/− mice after chronic cigarette smoke exposure. (*A*) Mean linear intercepts (MLI). Values are presented as mean ± SD (n = 6 for each group). In the lungs of SMP30Y/− mice exposed to cigarette smoke, MLI was significantly greater than the other groups (*$p < 0.05$). The MLI increased to 23.3% in the SMP30Y/− mice and to 5.4% for the SMP30Y/+ mice. The MLI in the SMP30Y/− mice exposed to air was significantly greater than that of the SMP30Y/+ mice exposed to air (†$p < 0.05$). (*B*) The destructive index (DI). Values are presented as mean ± SD (n = 6 for each group). In the lungs of the SMP30Y/− mice exposed to cigarette smoke, DI was increased more than 10% (*$p < 0.05$ compared with the other groups).

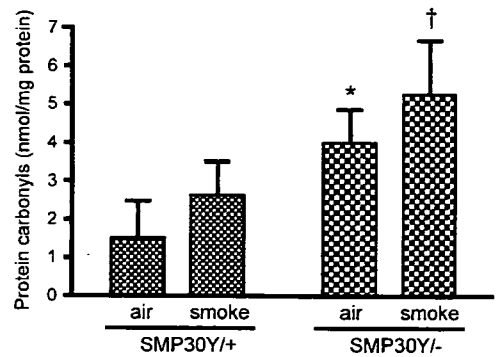

Figure 5. Protein carbonyls in the lungs of SMP30Y/+ and SMP30Y/− mice after chronic cigarette smoke exposure. Protein carbonyls in the lungs of SMP30Y/− mice were significantly greater in the air- and smoke-exposed groups than those of SMP30Y/+ mice (*$p < 0.05$ compared with SMP30Y/+ mice air-exposed group, and †$p < 0.05$ compared with SMP30Y/+ mice smoke-exposed group). Values are presented as mean ± SD (n = 6 for each group).

Our results indicate that the lack of a SMP30 molecule brings forth an endogenous mild oxidative stress situation in the lungs and makes the lungs highly susceptible to oxidative stress induced by smoke exposure even if exogenous oxidative stress is so mild that it does not generate oxidative proteins and lipids and up-regulate glutathione in BALF of the SMP30Y/+ mice. In this context, SMP30Y/− mice seem to be an excellent tool for investigating the pathophysiology of the lung associated with oxidant/antioxidant imbalance like smoke-induced emphysema and aging-related conditions like the senile lung.

The precise function of SMP30 in terms of oxidant and antioxidant balance remains undetermined. We demonstrated previously that SMP30 is localized in the nuclei in addition to the cytoplasm of cultured mouse hepatocytes and is similar in its amino acid sequence to bacterial and yeast RNA polymerases (28). Accordingly, SMP30 may regulate gene expression, and the lack of SMP30 may cause down-regulation of antioxidant enzymes. It has recently been reported that with gene targeting of the Nrf2 (nuclear factor, erythroid-derived 2, like 2), a transcription factor regulating gene expression involved in antioxidant defense, inflammation, and cellular apoptosis, plays an important role in the development of smoke-induced emphysema (29): $Nrf2^{-/-}$ mice were demonstrated to be extremely susceptible to cigarette smoke–induced emphysema after 6 mo of exposure. Glutathione is a potent antioxidant in the lungs and is highly concentrated in the epithelial lining fluid (24, 25). The transcription of the gene for α-glutamylcysteine synthetase, the rate-limiting enzyme for glutathione synthesis, is markedly up-regulated by chronic cigarette smoke exposure (30). Cigarette smoke–induced up-regulation of γ-glutamylcysteine synthetase has been reported to be mediated by the redox-sensitive transcription factor, activating protein-1 (31, 32). Although we did not directly measure enzyme activities, SMP30 seems not to be involved in the regulation of γ-glutamylcysteine synthetase because the glutathione content in BALF was markedly increase after 8 wk of smoke exposure in the SMP30Y/− mice. Moreover, the activity of glutathione reductase is not likely to be affected in the SMP30Y/− mice because the fraction of the oxidized form of glutathione is approximately 8% of the increased total glutathione content of the BALF. Because γ-glutamylcysteine synthetase and glutathione reductase are involved in the Nrf2 pathway (29), SMP30 may not have functional cross-talk with Nrf2. On the other hand, we previously reported lipid deposition and degeneration of mitochondria in the liver, kidney, and

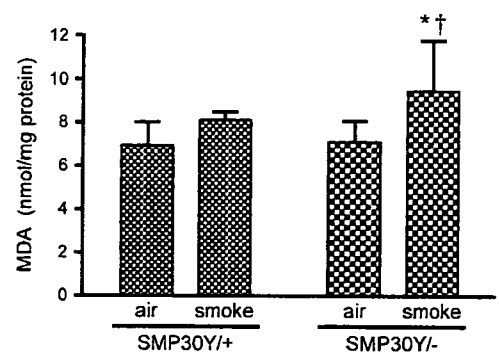

Figure 6. Malondialdehyde (MDA) in the lungs of SMP30Y/+ and SMP30Y/− mice after chronic cigarette smoke exposure. MDA was significantly increased in the lungs of SMP30Y/− mice exposed to cigarette smoke as compared with those of the air-exposed SMP30Y/+ (*$p < 0.05$) and SMP30Y/− (†$p < 0.05$) mice. Values are presented as mean ± SD (n = 6 for each group).

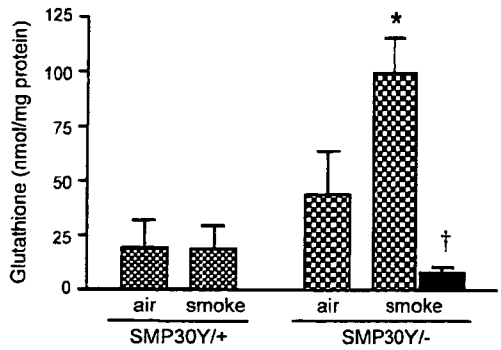

Figure 7. Total glutathione content in a bronchoalveolar lavage fluid (BALF) specimen of SMP30Y/+ and SMP30Y/− mice after chronic cigarette smoke exposure. Total glutathione content was significantly up-regulated in the SMP30Y/− mice exposed to cigarette smoke as compared with the other groups (*$p < 0.05$). Values are presented as mean ± SD ($n = 6$ for each group). †Oxidized glutathione was detected only in BALF from the smoke-exposed SMP30Y/− mice but not from the other groups (i.e., less than the detection limit). The amount of oxidized glutathione detected in the smoke-exposed SMP30Y/− mice was 7.91 nmol/mg protein (7.95% of total glutathione content).

submandibular gland of SMP30Y/− mice (8, 33, 34). The mitochondrion is speculated to be the main source of endogenous intracellular oxidant through a leak of an electron from the mitochondrial respiratory chain, but it has antioxidant enzymes (Mn-superoxide dismutase and glutathione peroxidase) that can attenuate oxidative stress. Recent studies have highlighted the important role of mitochondrial proteolytic enzymes in providing resistance to oxidative stress (35). Accordingly, the mitochondrial degeneration observed in the SMP30Y/−mice may be involved in the susceptibility of the lungs to oxidative stress. However, our preliminary electron microscopic analysis of the lungs did not detect structural abnormalities in the SMP30Y/− mice as compared with lungs of the SMP30Y/+ mice (data not shown). Further studies are needed to elucidate the precise role of SMP30 in oxidant/antioxidant balance by examining the gene expression profiles of the lungs from the SMP30Y/− mice with special reference to mitochondrial antioxidant enzymes and proteolytic enzymes.

We previously reported that SMP30Y/− is a novel murine model of senile lung because senile lungs develop spontaneous airspace enlargement without parenchymal destruction (5). This was confirmed in this study because SMP30Y/− mice showed significantly greater MLI at 3 mo of age than SMP30Y/+ mice. The SMP30Y/− mouse seems to be not only a murine model of senile lung but also a murine model of cigarette smoke–induced emphysema. SMP30Y/− mice are markedly susceptible to cigarette smoke, and smoke exposure for 8 wk was sufficient to develop cigarette smoke–induced pulmonary emphysema with marked airspace enlargement and parenchymal destruction. Although some animal models have been reported to develop cigarette smoke–induced pulmonary emphysema, most animal models required a longer period of cigarette smoke exposure, generally 6 or 7 mo, to generate smoke-induced emphysema. Because cigarette smoke–induced pulmonary emphysema in humans usually occurs in the elderly population, we considered that aging of the lung can be an important factor and should be incorporated into the experimental animal model for such condition. The effect of age on lung morphometry (36) and in the development of chronic cigarette smoke–induced lung pathology (37) has been reported. In BALB/cNNia mice, alveolar multiplication seemed to be completed by 38 d of age; interalveolar pore formation increased until 9 mo of age; and lung volume, alveolar surface area, and total volume of alveolar wall increased with age between 9 and 28 mo of age, which is postulated to be attributed to aging of the lungs (36). It was reported that in C57BL/6 mice, the older mice (8–10 mo of age) developed pathologic manifestations closely resembling pulmonary fibrosis and developed peribronchiolar and perivascular accumulations of lymphocytes and macrophages in the lungs after 9 mo exposure to cigarette smoke, whereas young mice (2 mo of age) revealed accumulations of inflammatory cells without fibrosis (37). Among other mice models for emphysema, the *klotho* mutant mouse and senescence-accelerated mouse (SAM) are unique due to their biological aging. The homozygous mutant *klotho* mice demonstrate a shorter life span and exhibit pulmonary emphysema, arteriosclerosis, osteoporosis, skin atrophy, and ectopic calcifications. However, the *klotho* mutant mice are distinct in developing pulmonary emphysema spontaneously without smoking (38). On the other hand, the SAM mice are the naturally occurring animal models for accelerated aging after normal development and maturation (39). We have recently reported that the SAMP1 mouse is capable of developing smoke-induced emphysema after 8 wk of cigarette smoke exposure. We also demonstrated that SAMP1 mice can be used for experiments involving therapeutic intervention because the development of smoke-induced emphysema was successfully prevented with concomitant administration of tomato juice, which contains a potent nutritional antioxidant, lycopene (14). In this context, SMP30Y/− mice further illustrate the significance of biological aging of the lungs in the development of cigarette smoke–induced pulmonary emphysema and may be considered as valuable animal models for smoke-induced emphysema.

Several mechanisms are likely to be involved in the development of cigarette smoke–induced pulmonary emphysema. An increase of oxidative stress to the lungs may be associated with many of the pathogenic processes, such as direct injury to lung cells, mucus hypersecretion, inactivation of antiproteases, enhancing lung inflammation through activation of redox-sensitive transcription factors, and apoptosis of lung cells (11). In the present study, chronic smoke exposure increased total cell count in SMP30Y/+ and SMP30Y/− mice. On the other hand, SMP30Y/− mice showed total protein level in BALF increased twofold from the baseline level after smoke exposure, whereas no change was detected in SMP30Y/+ mice. These findings may suggest that the inflammation in the lungs induced by chronic smoke exposure may be more pronounced in SMP30Y/− mice than in SMP30Y/+ mice, although we did not measure any other parameters of inflammation. Pulmonary emphysema can be generated without apparent inflammation, and it has recently been recognized that alveolar cell apoptosis could be one of the crucial process in emphysema: Direct instillation of activated caspase-3 (40) or vascular endothelial cell apoptosis resulting from the blockade of the vascular endothelial growth factor receptors (41) has been demonstrated to result in emphysema. As we reported previously that hepatocytes from SMP30Y/− mice are susceptible to apoptosis (7), we confirmed in this study that lungs cells are also susceptible to apoptosis triggered by oxidative stress. Accordingly, SMP30Y/− mice may be ideal animal models for cigarette smoke–induce emphysema in terms of investigating mutual interactions among apoptosis, oxidative stress, and inflammation, which is proposed as the mechanism for irreversible progression of parenchymal destruction (42, 43). Recently, up-regulation of lung ceramide, a second messenger lipid, has been reported to be a key pathogenic element in these mutual interactions (44). Because we have previously demonstrated that abnormal lipid metabolism occurs in the liver of the SMP30Y/− mice

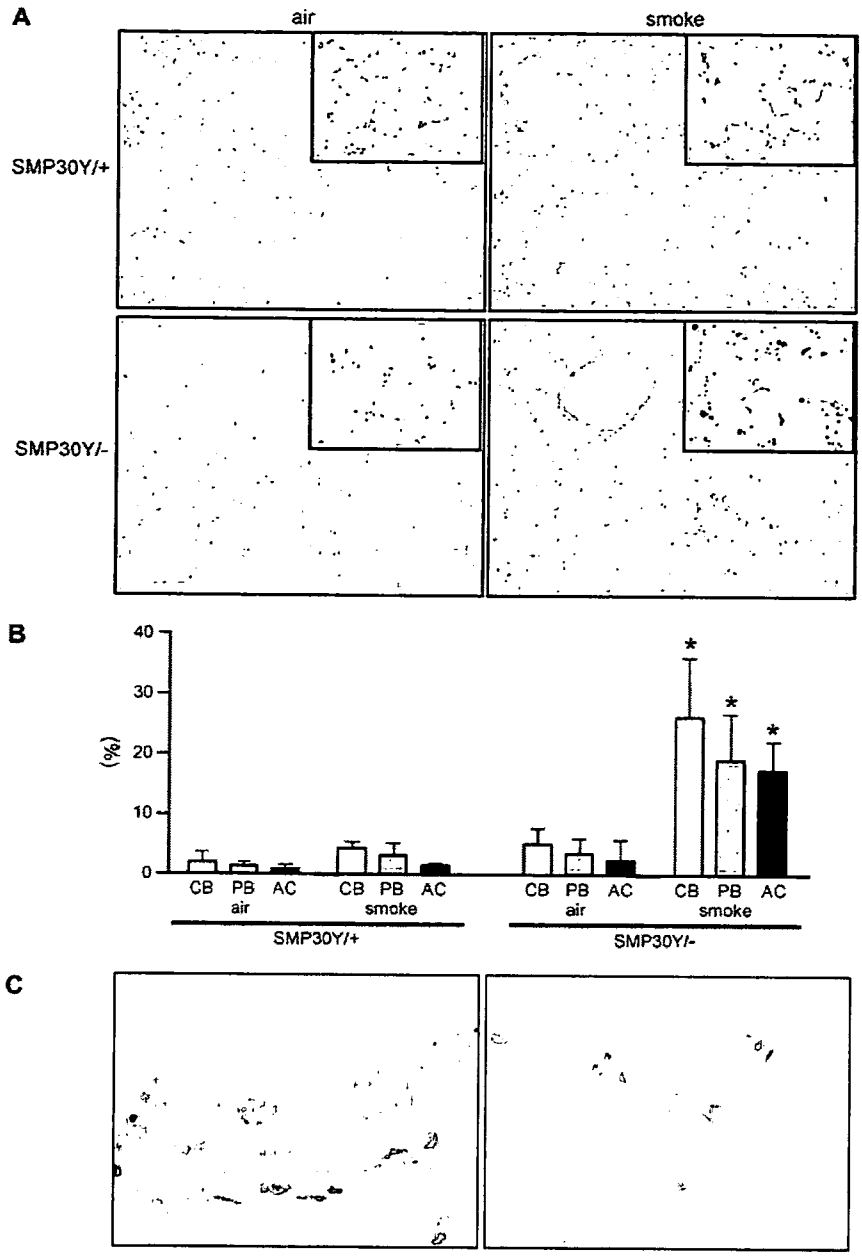

Figure 8. Immunohistochemical detection of apoptosis in the lungs of SMP30Y/+ and SMP30Y/− mice after cigarette smoke exposure. (*A*) Representative results of immunohistochemistry for single-stranded DNA (original magnification: ×50). *Insets* are magnified views of the alveolar region (×200). Note that positive immunostaining (nucleus stained *brown*) for DNA strand breaks was revealed in airway epithelial and alveolar wall cells in the lungs of SMP30Y/− mice after cigarette smoke exposure compared with the other groups. (*B*) Immunoreactive nuclei for anti–single-stranded DNA antibody were counted in three areas and expressed as the positive ratio (%) of total nuclei counted. AC = alveolar septal cells; CB = bronchial cells in the central airway; PB = bronchiolar cells adjacent to alveolar duct. The ratio of positively immunostained nuclei in all areas of the lungs of cigarette smoke–exposed SMP30Y/− mice was significantly higher than those of the other groups (*$p < 0.001$). Values are presented as mean ± SD ($n = 6$ for each group). (*C*) Representative results of immunohistochemistry for the activated caspase-3 in the lungs of the SMP30Y/− mice after cigarette smoke exposure (*left*: bronchial cells; *right*: alveolar septal cells; original magnification ×200). Positive reactions were identified in the lungs of cigarette smoke–exposed SMP30Y/− mice but were rarely seen in the lungs of the other groups.

(8), we need to examine whether SMP30 may be involved in the regulation of lung ceramide as the next step of our study.

Conflict of Interest Statement: None of the authors has a financial relationship with a commercial entity that has an interest in the subject of this manuscript.

Acknowledgment: The authors thank Dr. Toshio Kumasaka, Department of Pathology, Juntendo University, School of Medicine, for advice and technical help.

References

1. Fujita T, Uchida K, Maruyama N. Purification of senescence marker protein-30 (SMP30) and its androgen-independent decrease with age in the rat liver. *Biochim Biophys Acta* 1992;1116:122–128.
2. Fujita T, Shirasawa T, Uchida K, Maruyama N. Isolation of cDNA clone encoding rat senescence marker protein-30 (SMP30) and its tissue distribution. *Biochim Biophys Acta* 1992;1132:297–305.
3. Fujita T, Shirasawa T, Uchida K, Maruyama N. Gene regulation of senescence marker protein-30 (SMP30): coordinated up-regulation with tissue maturation and gradual down-regulation with aging. *Mech Ageing Dev* 1996;87:219–229.
4. Fujita T, Shirasawa T, Maruyama N. Isolation and characterization of genomic and cDNA clones encoding mouse senescence marker protein-30 (SMP30). *Biochim Biophys Acta* 1996;1308:49–57.
5. Mori T, Ishigami A, Seyama K, Onai R, Kubo S, Shimizu K, Maruyama N, Fukuchi Y. Senescence marker protein-30 knockout mouse as a novel murine model of senile lung. *Pathol Int* 2004;54:167–173.
6. Fujita T, Mandel JL, Shirasawa T, Hino O, Shirai T, Maruyama N. Isolation of cDNA clone encoding human homologue of senescence marker protein-30 (SMP30) and its location on the X chromosome. *Biochim Biophys Acta* 1995;1263:249–252.
7. Ishigami A, Fujita T, Handa S, Shirasawa T, Koseki H, Kitamura T, Enomoto N, Sato N, Shimosawa T, Maruyama N. Senescence marker protein-30 knockout mouse liver is highly susceptible to tumor necrosis factor-alpha- and Fas-mediated apoptosis. *Am J Pathol* 2002;161:1273–1281.
8. Ishigami A, Kondo Y, Nanba R, Ohsawa T, Handa S, Kubo S, Akita M, Maruyama N. SMP30 deficiency in mice causes an accumulation of